OPEN ACCESS

Original research

TNF-α drives pancreatic microcirculatory dysfunction via CD8$^+$ T cell-mediated endothelial injury in severe acute pancreatitis

Liang Shi,[1,2] Weiqi Li,[1,2] Duojiao Chen,[3] Boqiang Liu ,[1] Zihao Huang,[1,2] Chenqi Jin,[1,2] Lingfeng Ma,[4] Qiang Liu,[3] Bingzhi Dong,[1,2] Zhaoyuan Pan,[1,2] Lijun Du,[1,2] Lidan Hou,[1] Muxiong Chen,[1,2] Jinyan Xie,[2,5] Rongpan Bai ,[1,2] Hongcang Gu,[2,6] Di Wang,[7] Xin Yu,[2,8] Bo Shen,[1,2] Junbin Qian,[3,9] Hong Yu [1,2]

► Additional supplemental material is published online only. To view, please visit the journal online (https://doi.org/10.1136/gutjnl-2025-337183).

For numbered affiliations see end of article.

Correspondence to
Dr Hong Yu; blueyu000@zju.edu.cnDr Junbin Qian; dr_qian@zju.edu.cnDr Bo Shen; simpleshen@zju.edu.cn and Dr Xin Yu; xinxin_yu@zju.edu.cn

LS, WL and DC contributed equally.

Received 6 October 2025
Accepted 20 May 2026

Check for updates

© Author(s) (or their employer(s)) 2026. Re-use permitted under CC BY-NC. No commercial re-use. See rights and permissions. Published by BMJ Group.

To cite: Shi L, Li W, Chen D, *et al*. *Gut* Epub ahead of print: [*please include* Day Month Year]. doi:10.1136/gutjnl-2025-337183

ABSTRACT

Background Severe acute pancreatitis (SAP) is a life-threatening inflammatory disorder characterised by progressive multiorgan dysfunction. Direct investigation of human pancreatic tissue in SAP has been extremely limited, and effective targeted therapies are currently lacking.

Objective We sought to define the cellular and molecular mechanisms of SAP progression to identify actionable therapeutic targets.

Design Using rare pancreatic tissues from critically ill patients with SAP (n = 8), we constructed the first single-cell transcriptomic atlas of human SAP. Cellular compositional changes and intercellular communication were analysed to elucidate disease mechanisms. Findings were integrated with clinical data from a large patient cohort (n = 153) and validated through in vitro and in vivo studies in murine and porcine models.

Results We identified pancreatic microcirculatory failure as a central pathological event in SAP, driven by CD8$^+$ T cell-mediated endothelial injury. Mechanistically, tumour necrosis factor-alpha (TNF-α) upregulates UL16-binding proteins (ULBPs) on endothelial cells, activating the cytotoxic receptor NKG2D on infiltrating CD8$^+$ T cells and creating a feed-forward loop that amplifies microvascular damage. The TNF-α/ULBP/NKG2D axis correlated with clinical disease severity and microcirculatory dysfunction in patients. In preclinical models, inhibition of TNF-α or CD8$^+$ T cells preserved microvascular integrity, reduced tissue damage and improved survival.

Conclusion This study provides the comprehensive cellular map of human SAP and uncovers a pathogenic immune-endothelial circuit—orchestrated by the TNF-α/ULBP/NKG2D axis—that drives microcirculatory dysfunction. These findings establish a mechanistic rationale for targeting TNF-α as a potential therapeutic strategy in SAP.

WHAT IS ALREADY KNOWN ON THIS TOPIC

⇒ The incidence of severe acute pancreatitis (SAP) has steadily increased, imposing a significant burden on healthcare systems.
⇒ Microcirculatory disturbances and microvascular damage play a pivotal role in the onset and progression of SAP; however, the underlying cellular mechanisms remain unclear.
⇒ There is currently no specific drug to prevent or mitigate SAP pathophysiology process.

WHAT THIS STUDY ADDS

⇒ Infiltrating CD8$^+$ T cells drive pancreatic microcirculatory failure in SAP by directly targeting and killing endothelial cells via the NKG2D–UL16-binding proteins (ULBPs) axis.
⇒ Tumour necrosis factor-alpha (TNF-α) is a central mediator of this process, amplifying CD8$^+$ T cell cytotoxicity by inducing ULBPs expression on endothelium.
⇒ TNF-α is not only a biomarker of disease severity but also a promising therapeutic target for SAP.

HOW THIS STUDY MIGHT AFFECT RESEARCH, PRACTICE OR POLICY

⇒ Construction of the most comprehensive cellular landscape of human SAP to date, representing a foundational resource for future research.
⇒ Identification of cytotoxic CD8$^+$ T cell-mediated endothelial injury as a novel, targetable driver of microcirculatory failure in SAP.
⇒ Preclinical validation of anti-TNF-α therapy for SAP, enabling rapid clinical translation using repurposed, already-approved biologics.

INTRODUCTION

Acute pancreatitis (AP) is a digestive disorder caused by the abnormal activation of pancreatic enzymes, leading to acute inflammation and damage to pancreatic tissue.[1 2] While approximately 70% of AP cases follow a self-limiting course and resolve with short-term supportive care, around 20% progress to severe AP (SAP), a condition marked by pronounced systemic inflammation and multiorgan dysfunction.[3 4] Patients with SAP face significantly higher mortality rates, longer hospital stays and worse quality of life.[5] Despite ongoing research, there remains no specific drug to prevent or mitigate the pathophysiology processes of SAP,

Gut: first published as 10.1136/gutjnl-2025-337183 on 3 June 2026. Downloaded from http://gut.bmj.com/ on June 29, 2026 by guest. Protected by copyright, including for uses related to text and data mining, AI training, and similar technologies.

primarily due to the incomplete understanding of its intricate mechanisms.

One of the major challenges in pancreatitis research is a limited availability of patient samples obtained directly from inflamed pancreatic tissue, primarily due to the anatomical complexity of the pancreas and ethical constraints. As a result, current insights into AP are largely derived from various mouse models and patient blood tests. In recent years, single-cell RNA sequencing (scRNA-seq) has significantly advanced biomedical research. scRNA-seq analysis of peripheral blood mononuclear cells from patients with SAP has revealed distinct monocyte subpopulations as potential biomarkers and therapeutic targets.[6] Additionally, scRNA-seq studies in mouse models of AP have provided dynamic insights into disease progression.[7] However, a comprehensive analysis of the local cellular landscape within the pancreas of patients with SAP remains unexplored, posing a critical barrier to further advancements in SAP research.

Microcirculatory disturbances and microvascular damage play pivotal roles in the onset and progression of SAP, leading to local metabolite accumulation and exacerbating pancreatic necrosis, highlighting the critical importance of fluid resuscitation in clinical management.[8–11] In a porcine model of SAP, impaired microcirculation has been identified as the primary cause of reduced pancreatic tissue oxygenation and subsequent damage.[12] However, while systematic fluid resuscitation is closely linked to tissue microcirculation, the optimal resuscitation strategy remains a topic of debate in clinical practice.[13] This challenge may be addressed through a more refined understanding of the interplay between systemic circulation and pancreatic microcirculation, paving the way for more targeted therapeutic approaches.

During the pathophysiological progression of SAP, endothelial cell (EC) damage and increased vascular permeability lead to excessive capillary leakage, further aggravating tissue oedema and local ischaemia.[14–16] Consequently, researchers have actively been exploring approaches to restore microcirculatory function by targeting endothelial injury as a means to improve SAP outcomes.[17 18] Unfortunately, these efforts still remained in the preclinical stage, largely due to an incomplete understanding of the mechanisms underlying endothelial dysfunction in SAP.

In this study, we performed scRNA-seq on pancreatic tissues obtained from human patients with SAP, which, to our knowledge, represents the first report of the sequencing of human AP tissues. By using these rare and invaluable samples, we reconstructed the transcriptomic cellular landscape of human SAP and identified key factors influencing its pathophysiology. Furthermore, our findings underscore the critical role of $CD8^+$ T cells in driving the progressive failure of pancreatic microcirculation. Clinically, based on evidence from multiple models, we propose that anti-tumour necrosis factor-alpha (anti-TNF-α) therapy holds promise as a potential strategy to counteract this pathological process and improve outcomes in patients with SAP.

METHODS

Patients

The first cohort consisted of 8 patients with SAP and 13 patients with pancreatic tumours. Among the 13 patients with pancreatic tumour, 11 samples were obtained from Peng *et al* (GSA: CRA001160)[19] and 2 were collected at our centre. Patients underwent surgical treatment at our centre from August 2019 to August 2024. For the patients with pancreatic tumours, we collected normal pancreas samples at least 3 cm away from the tumour site. In contrast, the SAP samples were collected from patients with SAP who underwent distal pancreatectomy with splenectomy and debridement and drainage for pancreatic necrosis. These patients were not candidates for standard endoscopic or laparoscopic debridement procedures because of septic instability, extensive bacterial abdominal necrosis and complete discontinuity of the pancreas, as confirmed by radiological imaging. The SAP tissue samples were carefully collected from non-necrotic regions of the inflamed pancreas, as identified by the surgical team and verified by subsequent pathological examination. To prevent rapid degradation due to the specific characteristics of the pancreatic tissue, the samples were collected immediately after transection of the distal pancreas. All the samples were subjected to cell dissociation and scRNA sequencing within 2 hours.

The second cohort consisted of 153 patients with SAP who were hospitalised at Sir Run Run Shaw Hospital between October 2021 and June 2024. Blood samples for all laboratory determinations were collected uniformly within 6 hours of admission to the hospital. All patients met the diagnostic criteria for SAP, which included clinical evaluation of signs and symptoms, blood tests and imaging studies. All patients were admitted to the intensive care unit (ICU) because of organ failure and had acute physiology and chronic health evaluation II (APACHE II) scores ≥8.

Detailed materials and methods, including the experimental procedures and data analysis of scRNA-seq are provided in the online supplemental materials.

Patient and public involvement

Patients were not involved in the development of the research question and outcome measures.

RESULTS

Transcriptomic landscape of SAP generated by single-cell sequencing

Between 2019 and 2024, we successfully obtained eight pancreatic samples from patients with SAP who underwent distal pancreatectomy with splenectomy and debridement and drainage for pancreatic necrosis. These patients were ineligible for standard endoscopic or laparoscopic debridement procedures because of septic instability, extensive bacterial abdominal necrosis and complete discontinuity of the pancreas, as confirmed by radiological imaging. A clinical management process diagram of clinical management and detailed patient characteristics are provided (figure 1A–C, online supplemental figure S1A and table S1). Samples were carefully procured from non-necrotic regions of the inflamed pancreas, as identified by the surgical team and verified by subsequent pathological examination. To minimise degradation due to the inherent fragility of pancreatic tissue, samples were collected immediately after transection of the distal pancreas, followed by rapid tissue dissociation and scRNA-seq using established protocols.

For comparison, we also analysed 13 normal pancreatic tissue samples obtained from patients who underwent pancreatic tumour surgeries (sourced from our centre and publicly available databases, online supplemental table S2). Given the extensive necrosis of acinar cells, which could contribute to potential data contamination in surgical patients with SAP, we performed rigorous data cleaning for the scRNA-seq dataset (see the Methods section for details). After quality control and batch correction, a total of 167 076 cells, derived from both SAP and normal pancreatic tissues, were classified into 16 distinct major cell types and 49 subtypes, including parenchymal/stromal cells

Gut: first published as 10.1136/gutjnl-2025-337183 on 3 June 2026. Downloaded from http://gut.bmj.com/ on June 29, 2026 by guest. Protected by copyright, including for uses related to text and data mining, AI training, and similar technologies.

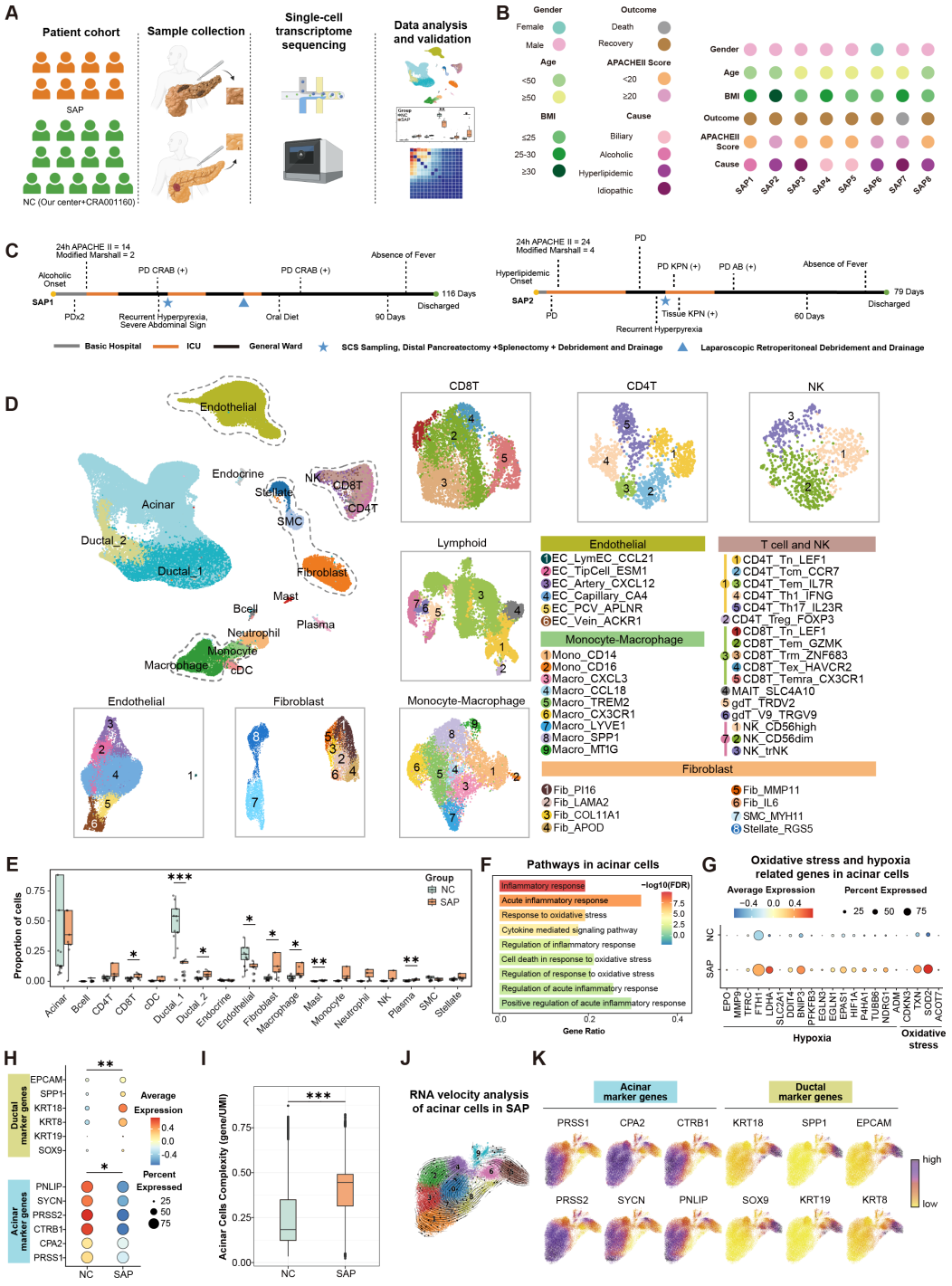

Figure 1 Transcriptomic landscape of SAP generated by single-cell sequencing. (A) Schematic overview of the scRNA-seq study design incorporating 8 SAP samples and 13 NC samples. (B) Clinical characteristics of the SAP patient cohort. (C) Process diagram of clinical management of two representative patients with SAP (SAP1 and SAP2). (D) UMAP projection of major cell lineages identified in pancreatic tissues. (E) Boxplots revealed the frequency of major cell compartments across NC and SAP groups (*p<0.05, **p<0.01, ***p<0.001, unpaired Student's t-test). (F) Top enriched terms from GO enrichment analysis related to oxidative stress and hypoxia of acinar cells in SAP group. (G) Dotplot of oxidative stress and hypoxia related genes for acinar cell between the NC and SAP groups. (H) Dotplot of additional marker genes for acinar and ductal cells in acinar cells between the NC and SAP groups (*p<0.05, **p<0.01, Wilcoxon rank-sum test). (I) Boxplot of transcriptional complexity (genes per UMI count) of acinar cells between the NC and SAP groups (***p<0.001, Wilcoxon rank-sum test). (J) RNA velocity pseudotime trajectory analysis of acinar cells. (K) Illustrating dynamic expression of acinar (*CPA2*, *PRSS1*, *CTRB1*, *PRSS2*, *SYCN* and *PNLIP*) and ductal (*KRT19*, *SOX9, KRT8, KRT18, SPP1* and *EPCAM*) marker genes along trajectories. AB, *Acinetobacter baumannii*; APACHE II, acute physiology and chronic health evaluation II; BMI, body mass index; CRAB, carbapenem-resistant *Acinetobacter baumannii*; cDC, conventional dendritic cell; EC, endothelial cell; FDR, false discovery rate; GO, Gene Ontology; ICU, intensive care unit; KPN, *Klebsiella pneumoniae*; NC, normal control; NK, natural killer; PD, peritoneal drainage; SAP, severe acute pancreatitis; scRNA-seq, single-cell RNA sequencing; SCS, single-cell sequencing; SMC, smooth muscle cell; Tcm, central memory T cells; Tem, effector memory T cells; Temra, terminally differentiated effector memory T cells; Tex, exhausted T cells; Th1, T helper 1 cell; Tn, naive T cells; Treg, regulatory T cell; Trm, tissue-resident memory T cells; UMAP, Uniform Manifold Approximation and Projection; UMI, unique molecular identifier.

Gut: first published as 10.1136/gutjnl-2025-337183 on 3 June 2026. Downloaded from http://gut.bmj.com/ on June 29, 2026 by guest. Protected by copyright, including for uses related to text and data mining, AI training, and similar technologies.

(acinar, ductal, endocrine, fibroblast and ECs), lymphoid cells (T, natural killer (NK) and B/plasma cells), mast cells and myeloid cells (monocytes, macrophages, neutrophils and dendritic cells) (figure 1D and online supplemental figure S1B,C). We quantified the proportional abundance of each cell type across all the samples in aggregate and for each individual sample (online supplemental figure S1D,E). This single-cell atlas of SAP is publicly accessible for exploration through an interactive web server (https://atlas.qian-lab.org/sap).

To identify potential key factors involved in SAP pathology, we compared the distribution of each cell type between the SAP and normal control (NC) groups. The results revealed an increase in $CD8^+$ T cells, type 2 pancreatic ductal epithelial cells (PDECs, Ductal_2), fibroblasts, macrophages, mast cells and plasma cells, along with a decrease in type 1 PDECs (Ductal_1) and ECs (figure 1E). Although the number of acinar cells, which are primarily subjected to intracellular autodigestion and contribute to tissue necrosis, did not change significantly, functional enrichment analysis revealed pronounced inflammatory and oxidative stress responses within these cells, along with signals of cell death (figure 1F and online supplemental figure S1F). Gene expression analysis further revealed an increased expression of genes related to oxidative stress and hypoxia (figure 1G). These findings indicate that acinar cells adopt a broadly inflammatory state, accompanied by strong responses to oxidative stress and hypoxia.[20–22]

In acinar cells, we observed a concerted downregulation of acinar marker expression, accompanied by an upregulation of ductal marker expression (figure 1H). Additionally, compared with the NC group, acinar cells from patients with SAP also exhibited increased transcriptional complexity, suggesting a shift in cell identity (figure 1I). RNA velocity analysis supported this phenotypic transition, demonstrating a trajectory from classic acinar states toward duct-like characteristics in SAP acinar cells (figure 1J,K, cluster 5). These findings confirm the presence of acinar-ductal metaplasia (ADM) in human AP samples, which is considered a crucial process in pancreatitis and a precursor to pancreatic cancer.[7 23 24]

Notably, we also observed a transition of ductal cells in SAP samples, specifically from type 1 to type 2 PDECs (figure 1E). Type 2 PDECs (Ductal_2) cells displayed activation of pathways linked to proinflammation, microenvironment remodelling and hypoxia (online supplemental figure S1G). Consistent with the finding of previous, type 2 PDECs are associated with cancer-related processes such as cell proliferation, migration and hypoxia responses, whereas type 1 cells are associated with normal pancreatic physiological functions.[19] This transition likely represents an adaptive response of ductal cells to inflammation, tissue damage and hypoxia during AP.

Together, these analyses characterised the basic cellular transcriptomic landscape of SAP, highlighting widespread inflammation, cell death, dynamic cellular transition and a hypoxic microenvironment, and pinpointing several key cell populations central to disease pathogenesis.

Microvasculature impairment drives microcirculatory failure in SAP

Cell type abundance analysis revealed a significant reduction of ECs in the SAP group compared with those in the NC group (figure 1E). Given the hypoxia signals observed in acinar cells, we further examined the condition of ECs in SAP. Subclustering of ECs identified six subtypes: lymphatic EC, tip cell, artery, capillary, postcapillary venule and vein (figure 2A and online supplemental figure S2A). Notably, a substantial decrease in capillaries was observed in SAP ($p<0.01$), suggesting a disruption of the pancreatic microvascular architecture that may ultimately lead to tissue hypoxia (figure 2B).[25 26] Immunofluorescence staining directly confirmed a significant loss of ECs in tissues of person with SAP (online supplemental figure S2B).

Pathway enrichment analysis revealed significant upregulation of death-associated pathways (eg, 'Regulation of cell death' and 'Programmed cell death') and immune activation signals (eg, 'Regulation of immune system process' and 'Response to cytokine') in ECs from patients with SAP (figure 2C). Additionally, vascular function-related pathway analysis confirmed significant endothelial dysfunction, particularly in capillary, indicating structural damage to the pancreatic vasculature (figure 2D,E and online supplemental figure S2C). Interestingly, we also detected signals indicating smooth muscle cell (SMC) damage within ECs, suggesting impaired vascular contractility in SAP tissues (figure 2D,E, right panel and online supplemental figure S2C, right panel).

To further investigate stromal-related vascular alteration, we characterised six fibroblast subtypes, SMCs and stellate cells in human SAP tissues (figure 2F and online supplemental figure S2D). We found a significant expansion of the adventitial (Fib_PI16), myofibroblastic (Fib_COL11A1), tissue-remodelling (Fib_MMP11) and inflammatory (Fib_IL6) fibroblast subsets in SAP, indicating a shift towards a profibrotic and inflammatory microenvironment (figure 2G and online supplemental figure S2E). Pseudotime trajectory analysis revealed that adventitial fibroblasts serve as progenitor cells, differentiating into three major lineages: adipogenic, tissue-remodelling and inflammatory fibroblasts (figure 2H), consistent with prior cross-tissue lineage models.[27] Notably, fibroblast differentiation in SAP was largely arrested at the progenitor stage, and successfully differentiated cells exhibited a pronounced bias toward the tissue-remodelling and inflammatory lineages (figure 2I). In contrast, the adipogenic lineage (Lineage 1), which is predominant in the normal pancreas, was suppressed. This was further evidenced by the strong activation of myofibroblast programmes (eg, *COL1A1*, *POSTN*; figure 2J and online supplemental figure S2F), aligning with previous findings.[7] Moreover, expression of critical inflammatory mediators (eg, *IL6*, *CCL5*) was also upregulated across tissue-remodelling and inflammatory lineages (figure 2K).

Meanwhile, we observed a marked reduction of SMCs in patients with SAP (figure 2G). These remaining SMCs underwent phenotypic switching, evidenced by loss of SMC identity marker (eg, *ACTA2*, *MYH11*) expression and increased expression of myofibroblast-associated markers (eg, *COL1A1*, *TAGLN*) (figure 2L). This transition likely exacerbates local microcirculatory dysfunction.[28] The consequent disruption of vascular contractility was supported by the downregulation of contraction-related gene signatures in SMCs (online supplemental figure S2G) and immunostaining revealing pronounced structural uncoupling between ECs and vascular SMCs in human SAP tissues (figure 2M). This finding demonstrates a fundamental defect in vascular wall integrity.

As a potential consequence of dysfunctional vasculature, we confirmed elevated hypoxia scores in acinar cells (figure 2N), as well as a broad increase of HIF-1α staining in SAP tissues (figure 2P), suggesting that hypoxia is a key manifestation of SAP microcirculatory failure. Analysis of scRNA-seq data from a murine AP model (GSE235874) also revealed hypoxic response of acinar cells (figure 2O).[7] However, this hypoxic state was rapidly resolved within 24 hours, failing to recapitulate the sustained hypoxia seen in human SAP tissues. To address this limitation, we established a murine model of sustained injury via continuous

Gut: first published as 10.1136/gutjnl-2025-337183 on 3 June 2026. Downloaded from http://gut.bmj.com/ on June 29, 2026 by guest. Protected by copyright, including for uses related to text and data mining, AI training, and similar technologies.

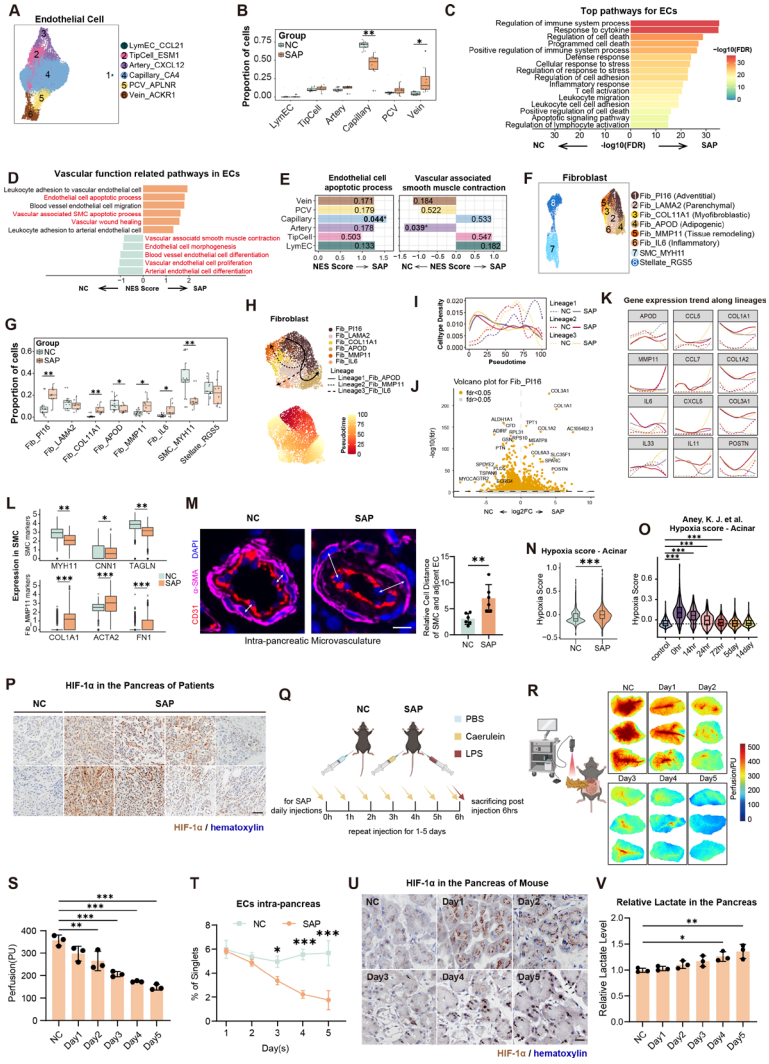

Figure 2 Pancreatic microvasculature impairment drives microcirculatory disturbance in SAP. (A) UMAP of pancreas ECs from the NC and SAP groups. (B) Boxplots revealing relative abundance of ECs across different groups (*p<0.05, **p<0.01, unpaired Student's t-test). (C) Top enriched terms from GO enrichment analysis of differentially expressed genes in ECs in SAP group. (D) GSEA analysis showed vascular function related pathways in ECs. Pathways related to vascular injury and repairment were highlighted in red. (E) GSEA analysis showed EC apoptotic process pathway (left panel) and vascular associated smooth muscle contraction pathway (right panel) in different groups (labelled with p value *p<0.05, x-axis: NES score from GSEA analysis). (F) UMAP plot of pancreas fibroblasts, SMCs and stellate cells from NC and SAP groups. (G). Boxplots revealing relative abundance of fibroblasts across different groups (*p<0.05, **p<0.01, ***p<0.001, unpaired Student's t-test). (H) Trajectory analysis revealed three differentiation lineages of fibroblasts (up panel), with inferred differentiation pseudotime (bottom panel). (I) The density plots showing the relative number of fibroblasts of specific lineage, separately for NC (dashed line) versus SAP (solid line), along the differentiation pseudotime. (J) Volcano plot showing differentially expressed genes of Fib_PI16 between NC and SAP. (K) Expression of inflammatory (*IL6*, *CCL5*) across the tissue-remodelling and inflammatory fibroblast lineages in SAP. (L) Boxplots showing the loss of SMC identity markers (*ACTA2*, *MYH11*) and gain of myofibroblast markers (*COL1A1*, *TAGLN*) in SAP SMCs, indicating phenotypic switching (*p<0.05, **p<0.01, ***p<0.001, Wilcoxon rank-sum test). (M) (Left) Immunofluorescence staining of CD31 (red, ECs) and α-SMA (pink, SMCs) in human pancreas samples. DAPI (blue) was used to stain the nucleus. White arrows indicate sites of EC-SMC uncoupling. Scale bars, 10 µm. (Right) Quantitative analysis of the relative distance between ECs and SMCs (**p<0.01, unpaired Student's t-test). (N) Hypoxia scores of acinar cells from scRNA-seq data in NC and SAP groups (***p<0.001, Wilcoxon rank-sum t-test). (O) Dynamic changes in acinar cell hypoxia scores from a murine acute pancreatitis model over time (***p<0.001; Wilcoxon rank-sum test). The scRNA-seq data sourced from Aney, K J *et al.* (P) Representative IHC images for HIF-1α (brown) in human NC and SAP pancreatic tissues. Nuclei are counterstained with haematoxylin (blue). Scale bars, 50 µm. (Q) Schematic of the sustained murine SAP model induced by caerulein and LPS administration. (R) Representative LSCI maps of pancreatic blood perfusion in mice. (S) Quantification of pancreatic perfusion from LSCI over time (mean±SD; **p<0.01, ***p<0.001; unpaired Student's t-test). (T) Proportion of $CD45^{-}CD31^{+}$ ECs in murine pancreatic tissue over time, as measured by flow cytometry (mean±SD, *p<0.05, ***p<0.001, two-way ANOVA). (U) Representative IHC images for HIF-1α (brown) in murine pancreatic tissues over time. Black arrows indicate nuclei with positive staining. Scale bars, 20 µm. (V) Relative lactate levels in murine pancreatic tissue over time, normalised to total protein (mean±SD, *p<0.05, **p<0.01, one-way ANOVA). ANOVA, analysis of variance; DAPI, 4′,6-diamidino-2-phenylindole; ECs, endothelial cells; FDR, false discovery rate; GO, Gene Ontology; GSEA, Gene Set Enrichment Analysis; IHC, immunohistochemistry; IL, interleukin; LPS, lipopolysaccharide; LSCI, laser speckle contrast imaging; LymEC, lymphatic endothelial cell; NC, normal control; NES, normalised enrichment score; PBS, phosphate-buffered saline; PCV, postcapillary venule; PU, perfusion units; SAP, severe acute pancreatitis; scRNA-seq, single-cell RNA sequencing; SMC, smooth muscle cell; UMAP, Uniform Manifold Approximation and Projection.

Gut: first published as 10.1136/gutjnl-2025-337183 on 3 June 2026. Downloaded from http://gut.bmj.com/ on June 29, 2026 by guest. Protected by copyright, including for uses related to text and data mining, AI training, and similar technologies.

caerulein and LPS exposure (figure 2Q and online supplemental figure S2H–M), which induced progressive pathophysiological changes, including prolonged microcirculatory dysfunction. Laser speckle contrast imaging (LSCI) confirmed a marked deterioration in the pancreatic microcirculatory perfusion of mice that persisted for at least 5 days (figure 2R,S). This was accompanied by a significant reduction in $CD45^{-}CD31^{+}$ ECs, further supporting sustained endothelial damage (figure 2T). In response, HIF-1α protein upregulation was prolonged up to 5 days (figure 2U). Consistently, we detected progressive lactate accumulation within the pancreas, a hallmark of hypoxic condition and microcirculatory failure (figure 2V).

These findings highlight pancreatic microvasculature impairment as a key driver of microcirculatory failure and hypoxia in SAP, representing a pivotal mechanism in disease progression.

Single-cell sequencing reveals the increase of $CD8^{+}$ Temra cells in SAP

Among the significantly enriched cell types in SAP (figure 1E), macrophages have long been recognised as key mediators of innate immune responses in pancreatitis.[7 29] However, the role of $CD8^{+}$ T cells in non-autoimmune pancreatitis remains unclear and controversial.[30] Immunofluorescence staining corroborated the marked infiltration of macrophages and $CD8^{+}$ T cells in tissue samples from our patients with SAP (online supplemental figure 3A).

Next, we performed unsupervised clustering of monocyte-macrophages, identifying two monocyte subtypes and seven macrophage subtypes (figure 3A and online supplemental figure S3B). Notably, we observed a significant expansion of the proinflammatory (Macro_CXCL3) and stress-associated (Macro_MT1G) macrophage subsets concurrent with a reduction in two other populations (Macro_LYVE1 and Macro_CX3CR1) (figure 3B). Importantly, the perivascular resident macrophages (Macro_LYVE1) function to maintain vascular structural homeostasis and resolve inflammation.[31] The reduction in this protective subset in SAP represents a loss of this critical function, thereby likely exacerbating microcirculatory and endothelial dysfunction.

As key mediators of the innate immune response, macrophages in SAP are involved in pancreatic inflammation, local stress responses and infection defence, as indicated by pathway enrichment analysis (figure 3C). However, these macrophages also exhibited elevated anti-inflammatory scores and a shift toward an M2-like phenotype (figure 3D and online supplemental figure S3C). This duality underscores the complex and context-dependent role of macrophages in pancreatitis, highlighting the need for further investigation.[7 32]

For T/NK cells, we identified a total of 17 distinct subtypes (figure 3E and online supplemental figure S3D). Overall, we observed a significant expansion of central memory T cells, T helper 1 cells and regulatory T cells, indicating an inflammatory state likely driven by prolonged infection in pancreas (figure 3F). Concurrently, the reduction in $CD8^{+}$ tissue-resident memory T cells, along with the increase in exhausted T cells (Tex), suggests a state of immune exhaustion within the local microenvironment at this stage.

Notably, pathway enrichment analysis revealed a highly activated status of $CD8^{+}$ T cells in SAP samples, suggesting potentially enhanced cytotoxic functions (figure 3G). Among these cells, terminally differentiated effector memory $CD8^{+}$ T cells (Temra)—which are phenotypically distinct from $PD\text{-}1^{+}$ Tex (online supplemental figure S3E,I)—were significantly increased in SAP tissues (figure 3F and online supplemental figure S3F). These cells were activated and exhibited high cytotoxic potential, implicating them in local inflammation and immune modulation in SAP (figure 3H and online supplemental figure S3G). Immunofluorescence staining also confirmed the accumulation of $CD8^{+}CD45RA^{+}CCR7^{-}$ Temra cells exhibiting high GZMB expression in SAP pancreatic tissues (online supplemental figure S3H).

To further delineate the differentiation landscape of $CD8^{+}$ T cells, we performed pseudotime trajectory analysis using Slingshot, with $CD8^{+}$ naive T cells designated as the root state. This analysis revealed three major differentiation lineages (figure 3I,J), which is consistent with patterns observed in other diseases.[33 34] Interestingly, $CD8^{+}$ Temra lineage (Lineage 3) emerged as the predominant trajectory in SAP samples ($p<0.01$), suggesting a pivotal role for Temra cells in disease progression (figure 3K). Moreover, trajectory-based analysis revealed a progressive increase in the expression of cytotoxic mediators (eg, *GZMB, PRF1*) and inflammatory genes (eg, *TNF*, *TNFRSF1A*) along the Temra lineage, underscoring the dynamic functional shifts in $CD8^{+}$ T cells during SAP progression (figure 3L and online supplemental figure S3I).

Overall, these findings provide a comprehensive characterisation of the pancreatic immune landscape in human SAP. Interestingly, the distribution of $CD8^{+}$ T cells and the dynamic shifts in their subtypes strongly indicate an enhanced cytotoxic response to local inflammatory events, a phenomenon that has rarely been reported in previous animal model studies.[30]

Intrapancreatic $CD8^{+}$ T cells impair ECs via increased quantity and activity

Given the extensive EC damage observed in our analysis, we sought to identify the key components driving this pathological process and evaluate their potential as therapeutic targets. Pathway enrichment analysis of ECs from patients with SAP revealed upregulated signals related to immunocyte adhesion and activation (figure 2C and online supplemental figure S4A). Moreover, intercellular communication analysis revealed that $CD8^{+}$ T cells were the most prominent immune cell type that interacted with ECs (figure 4A). Immunofluorescence staining of pancreatic tissue from patients with SAP further demonstrated significant perivascular accumulation of $CD8^{+}$ T cells, which were predominantly localised around ECs rather than infiltrating into the pancreatic parenchyma (figure 4B).

As previously mentioned, the role of $CD8^{+}$ T cells in AP remains unclear.[30] However, in our human SAP samples, $CD8^{+}$ T cells were robustly activated, as evidenced by increased cytotoxicity, elevated cytokine release and enhanced degranulation capacity (figure 4C, left panel and online supplemental figure S4B, left panel). A similar hyperactive phenotype was observed in Temra cells (figure 4C, right panel and online supplemental figure S4B, right panel).

Traditional AP or SAP models often employ early sampling time points (6 hours–12 hours postinduction), which may not capture the full extent of $CD8^{+}$ T cell infiltration and function. In contrast, our extended SAP murine model (figure 2Q) revealed that intrapancreatic $CD8^{+}$ T cells began to increase on Day 3 and continued to accumulate as SAP progressed (online supplemental figure S4C and online supplemental figure S4H–M). Functionally, both $CD8^{+}$ T cells and Temra cells from SAP mice exhibited a progressive increase in activation over time, which is consistent with the findings in human (figure 4D and online supplemental figure S4D,E). Analysis of scRNA-seq data from a murine AP

Gut: first published as 10.1136/gutjnl-2025-337183 on 3 June 2026. Downloaded from http://gut.bmj.com/ on June 29, 2026 by guest. Protected by copyright, including for uses related to text and data mining, AI training, and similar technologies.

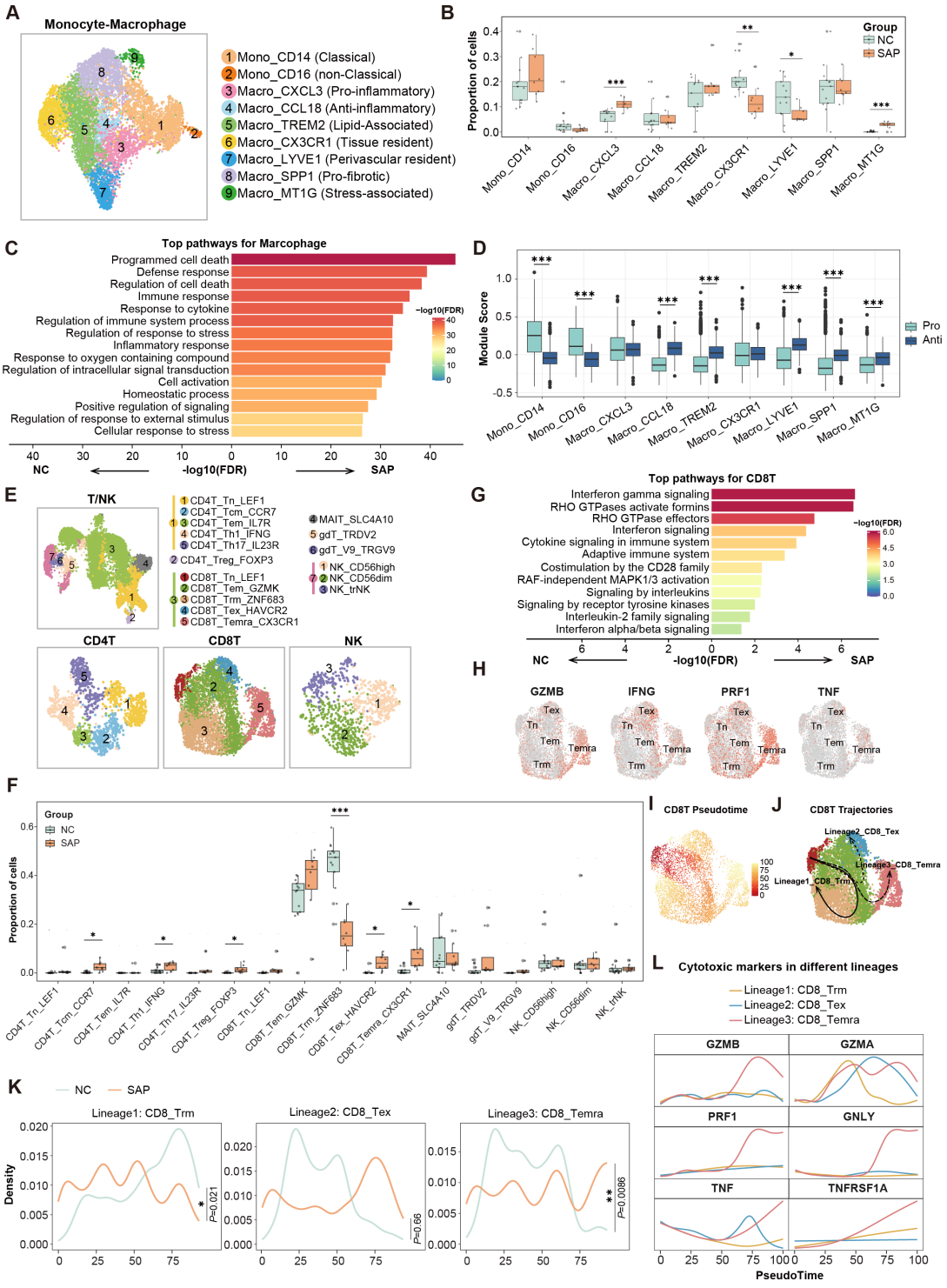

Figure 3 Single-cell sequencing reveals elevated CD8$^+$ Temra cells in SAP. (A) UMAP plot of pancreas monocyte and macrophage from NC and SAP groups. (B) Boxplots showing the frequency of monocyte and macrophage subpopulations across different groups (*p<0.05, **p<0.01, ***p<0.001, unpaired Student's t-test). (C) Top enriched terms from GO enrichment analysis of differentially expressed genes in SAP macrophages. (D) The proinflammatory and anti-inflammatory score of monocytes and macrophages in SAP group (***p<0.001, Wilcoxon rank-sum test). (E) UMAP plot of pancreas lymphoid cell from NC and SAP groups. (F) Boxplots showing the frequency of lymphoid cell subpopulations across groups (*p<0.05, ***p<0.001, unpaired Student's t-test). (G) Top enriched terms from REACTOME enrichment analysis of differentially expressed genes in SAP group CD8$^+$ T cells. (H) Expression levels of cytotoxic marker genes (*GZMB, IFNG*, *PRF1*, *TNF*) in all CD8$^+$ T cells on UMAP. (I) Trajectory analysis of pancreatic CD8$^+$ T cells with pseudotime annotation. (J) Trajectory analysis of all CD8$^+$ T cells showing three lineages. (K) CD8$^+$ T cell dynamics along three trajectories compared between NC and SAP groups (*p<0.05, **p<0.01, unpaired Student's t-test). (L) The expression dynamics of cytotoxic marker genes in three CD8$^+$ T cell lineages along pseudotime. FDR, false discovery rate; GO, Gene Ontology; NC, normal control; NK, natural killer; SAP, severe acute pancreatitis; Tcm, central memory T cells; Tem, effector memory T cells; Temra, terminally differentiated effector memory T cells; Tex, exhausted T cells; Th1, T helper 1 cell; Tn, naive T cells; TNF, tumour necrosis factor; Treg, regulatory T cell; Trm, tissue-resident memory T cells; UMAP, Uniform Manifold Approximation and Projection.

Gut: first published as 10.1136/gutjnl-2025-337183 on 3 June 2026. Downloaded from http://gut.bmj.com/ on June 29, 2026 by guest. Protected by copyright, including for uses related to text and data mining, AI training, and similar technologies.

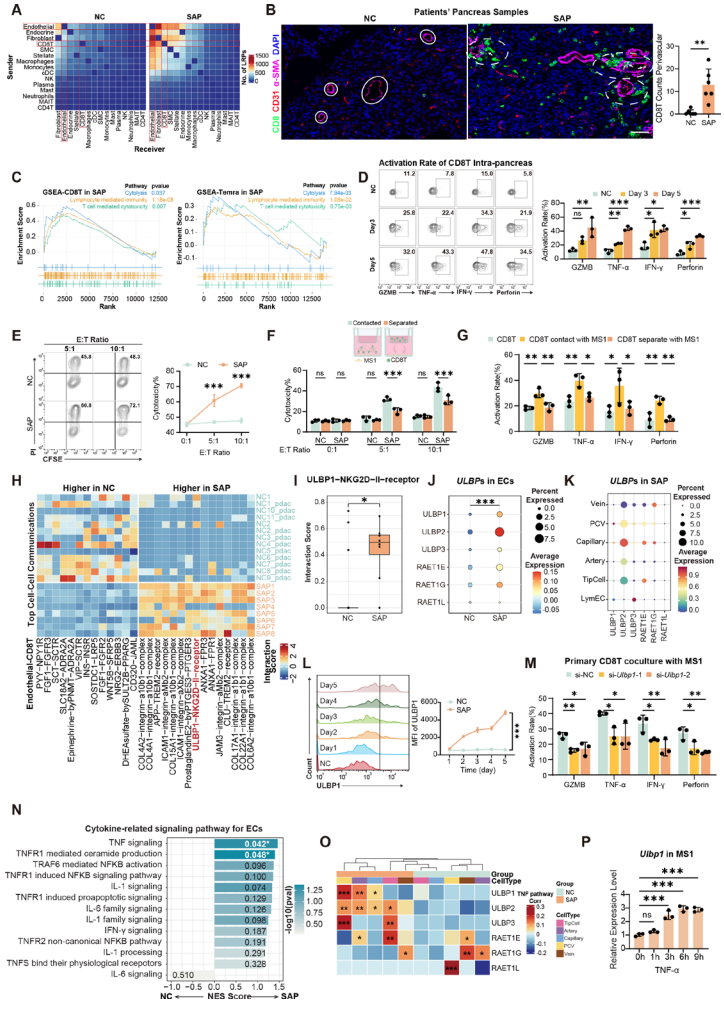

Figure 4 TNF-α-Induced NKG2D–ULBP Signalling Drives CD8$^+$ T cell-mediated EC damage. (A) Cell-–cell communication analysis identified CD8$^+$ T cell and EC interaction as the most frequent immune-stromal crosstalk. (B) Immunofluorescence staining of CD31 (red, endothelial), CD8 (green, CD8$^+$ T cell) and α-SMA (pink, SMC) in patients' pancreas samples (NC vs SAP, left panel). DAPI (blue) was used to stain the nucleus. Intact (solid white circles) and damaged (dashed circles) vessels are indicated; infiltrating CD8$^+$ T cells marked by arrows in SAP. (Scale bars, 50 µm.) The counts of CD8$^+$ T cell perivascular were quantified (right panel, mean±SD, **p<0.01, unpaired Student's t-test). (C) GSEA analysis showed the cytotoxicity-related pathways were activated in CD8$^+$ T cells (left panel) and Temra cells (right panel) in SAP group. (D) The activation rate (GZMB, TNF-α, IFN-γ and perforin) of CD8$^+$ T cell in mouse pancreas samples between NC and SAP in different days detected by flow cytometry. Representative flow cytometry images were shown (left panel). The activation rate of CD8$^+$ T cell was quantified (right panel, mean±SD, ns, not significant, *p<0.05, **p<0.01, ***p<0.001, one-way ANOVA test). (E) Primary pancreatic endothelial cells isolated by FACS were subjected to in vitro cytotoxicity assays using primary CD8$^+$ T cell at various E:T ratios. Representative flow cytometry images were shown (left panel). The cytotoxicity rate was quantified (right panel, mean±SD, ***p<0.001, two-way ANOVA test). (F) MS1 cells were co-cultured with primary CD8$^+$ T cells on either side of a 0.4 µm transwell as depicted at various E:T ratios and quantified the cytotoxicity after 24 hours of co-culture as cytotoxicity assays (mean±SD, ns, not significant, ***p<0.001, two-way ANOVA test). (G) The activation rate (GZMB, TNF-α, IFN-γ and perforin) of primary CD8$^+$ T cell in mouse pancreas co-cultured for 24 hours with MS1 or not and whether their contacted detected by flow cytometry. E:T ratio was 5:1 (mean±SD, *p<0.05, **p<0.01, one-way ANOVA test). (H) Top ligand–receptor pairs for CD8$^+$ T cell and ECs crosstalk. (I) ULBP1–NKG2D interaction scores in NC versus SAP (*p<0.05, Wilcoxon rank-sum test). (J) Dotplot showed the expression of ULBP family (*ULBP1-3*, *RAET1E*, *RAET1G* and *RAET1L*) in ECs between the NC and SAP groups (***p<0.001, Wilcoxon rank-sum test). (K) Dotplot showed the expression of ULBP family (*ULBP1-3*, *RAET1E*, *RAET1G* and *RAET1L*) in subpopulations of ECs in SAP group. (L) MFI of ULBP1 in ECs (CD45$^-$CD31$^+$) in mouse pancreas tissue between NC and SAP in different days detected by flow cytometry (left panel) and quantitative analysis (right panel) (mean±SD, ***p<0.001, two-way ANOVA test). (M) The activation rate (GZMB, TNF-α, IFN-γ and perforin) of primary CD8$^+$ T cell in mouse spleen co-cultured with si-NC MS1, si-*ULBP1*-1 MS1 or si-*ULBP1*-2 MS1 detected by flow cytometry. E:T ratio was 5:1 (mean±SD, *p<0.05, **p<0.01, one-way ANOVA test). (N) GESA analysis showing cytokine-related signalling pathway for SAP ECs. (O) Heatmap showing the correlation between expression level of ULBP family genes and TNF pathway in subpopulations of ECs (*p<0.05, **p<0.01, ***p<0.001, unpaired Student's t-test). (P) Relative mRNA expression level of *ULBP1* in MS1 cells treated with TNF-α (10 ng/mL) (mean±SD, ns, not significant, ***p<0.001, one-way ANOVA test). ANOVA, analysis of variance; cDC, conventional dendritic cell; CFSE, carboxyfluorescein succinimidyl ester; DAPI, 4′,6-diamidino-2-phenylindole; ECs, endothelial cells; E:T, effector-to-target; FACS, fluorescence-activated cell sorting; GSEA, Gene Set Enrichment Analysis; IFN-γ, interferon-gamma; IL, interleukin; LPR, ligand–receptor pairs; LymEC, lymphatic endothelial cell; MFI, mean fluorescence intensity; mRNA, messenger RNA; NC, normal control; NES, normalized enrichment score; NK, natural killer; PCV, postcapillary venule; PI, propidium iodide; SAP, severe acute pancreatitis; SMC, smooth muscle cell; Temra, terminally differentiated effector memory T cells; TNF-α, tumour necrosis factor-alpha; ULBP1, UL16-binding protein 1.

Gut: first published as 10.1136/gutjnl-2025-337183 on 3 June 2026. Downloaded from http://gut.bmj.com/ on June 29, 2026 by guest. Protected by copyright, including for uses related to text and data mining, AI training, and similar technologies.

model (GSE235874) revealed that $CD8^+$ T cell expression of cytokines and cytotoxic effectors was elevated during the acute inflammatory phase but diminished during recovery period (online supplemental figure S4F).

Next, we performed in vitro cytotoxicity assays. $CD8^+$ T cells were isolated from SAP mice and co-cultured with primary ECs isolated from control mouse pancreas. These assays demonstrated significantly enhanced cytotoxicity of SAP-derived $CD8^+$ T cells against primary ECs (figure 4E). A similar increase in cytotoxic activity was observed when using the immortalised mouse pancreatic EC line MS1 (online supplemental figure S4G), confirming that this $CD8^+$ T cell–EC interaction is a consistent and conserved feature. Considering previous evidence that ECs can act as T cell activators, especially under inflammatory conditions,[35] we employed a micropore membrane system with 0.4 µm transwell plates to separate $CD8^+$ T cells from ECs, thereby blocking direct contact. The resulting assay showed that direct cell–cell contact significantly amplified the cytotoxic effect of $CD8^+$ T cells on ECs, both in cytotoxicity assay and $CD8^+$ T cell activation analyses (figure 4F,G).

Collectively, these findings strongly suggest that increased infiltration and hyperactivation of $CD8^+$ T cells contribute to local microcirculatory disruption and tissue hypoxia in SAP through direct cytotoxic effects on ECs.

NKG2D–ULBP signalling mediates $CD8^+$ T cell-driven EC damage

To elucidate the mechanisms underlying the selective $CD8^+$ T cell targeting of ECs and the role of direct contact in amplifying cytotoxicity, we conducted a cell–cell communication analysis. The results revealed significantly upregulated receptor–ligand pairs between ECs and $CD8^+$ T cells in SAP, including NKG2D–UL16-binding proteins (ULBPs) (figure 4H). While several adhesion-related pairs (eg, collagen-integrin) suggested a role for ECs in recruiting $CD8^+$ T cells, other pairs like ANXA1-FPR1/3 and CLU-TREM2—which have reported immunosuppressive functions.[36 37] Moreover, *FPR1/3* and *TREM2* were predominantly expressed by macrophages instead of $CD8^+$ T cells (online supplemental figure S5A), which was unlikely to explain EC-induced $CD8^+$ T cell activation and cytotoxicity. In contrast, the NKG2D–NKG2DL axis, which is known to sustain the cytotoxic activity of $CD8^+$ T cells against major histocompatibility complex-I-negative tumours,[38] emerged as a strong candidate. NKG2D is an activating receptor expressed on immune cells, including NK cells, γδ T cells and $CD8^+$ T cells and plays a critical role in immune surveillance by enabling the recognition and clearance of virus-infected, stressed or malignant cells.[38–40] Its ligands, the ULBPs, are minimally expressed under homeostasis but are potently upregulated by cellular stress, inflammation or malignancy.[40–42]

Guided by this analysis, we investigated the NKG2D–ULBPs axis in SAP (figure 4H,I). scRNA-seq confirmed high *NKG2D* expression in SAP-derived Tex cells and Temra cells (online supplemental figure S5B). Strikingly, analysis of ULBP expression revealed its specific and pronounced upregulation in ECs from patients with SAP (figure 4J and online supplemental figure S5C). Among endothelial subpopulations, capillary showed the highest ULBP expression (figure 4K), which is consistent with their increased levels of apoptosis (figure 2E, left panel).

Given that ULBP1 is the primary functional murine ortholog of the human ULBP family,[43] we focused on it for our in vivo validation. ECs were sorted from the pancreas of mice with SAP using fluorescence-activated cell sorting, and transcriptomic analysis confirmed a significant upregulation of *Ulbp1* expression (online supplemental figure S5D). Concurrently, membrane–bound ULBP1 levels were found to increase over time in the SAP model (figure 4L).

Our previous transwell assays had already suggested that direct cell–cell contact enhances the cytotoxic effect of $CD8^+$ T cells on ECs (figure 4F,G). To determine whether the NKG2D–ULBPs axis mediated this effect, we knocked down or blocked ULBP1 in mouse ECs using a ULBP1 small interfering RNA or an NKG2D-neutralising antibody. Both approaches significantly diminished the $CD8^+$ T cell-mediated cytotoxic enhancement (figure 4M and online supplemental figure S5E).

To validate the NKG2D–ULBP1 axis in vivo, we administered anti-mouse NKG2D antibodies in a continuous injection-induced SAP mouse model (online supplemental figure S5F; n=10). As expected, mice treated with anti-NKG2D antibodies exhibited reduced weight loss and lower mortality rates (online supplemental figure S5G,H). After 8 days of observation, the surviving mice were sacrificed for further analysis. Histological scoring revealed significant reduction in pancreatic oedema, necrosis and immune infiltration in the treatment group (online supplemental figure S5I). Serum analyses confirmed corresponding decreases in amylase, interleukin (IL)-6 and IL-1β levels (online supplemental figure S5J–L). Additionally, the treatment group showed decreased serum and pancreatic lactate levels, indicating improved tissue oxygenation and perfusion (online supplemental figure S5M–O).

We further validated our findings using a public scRNA-seq dataset from a mouse AP model. In this short-term model, the ULBP1–NKG2D interaction score, *Nkg2d* expression in $CD8^+$ T cells and *Ulbp1* expression in ECs were all markedly upregulated, peaking at 24 hours before declining thereafter (online supplemental figure S5P–R).

In summary, $CD8^+$ T cells are further activated by pancreatic ECs through NKG2D–ULBP signalling in SAP, contributing to EC injury and microvascular disruption.

TNF-α induces ULBP upregulation via PERK-eIF2α-ATF4 axis in endothelial cells during SAP

Since ULBPs are known to be induced by inflammatory mediators such as cytokines, we next analysed cytokine-associated pathways in ECs using human SAP scRNA-seq data. Both Gene Set Enrichment Analysis and pathway enrichment analyses revealed marked activation of TNF-related pathways in pancreatic ECs from patients with SAP compared with controls (figure 4N and online supplemental figure S6A). Moreover, TNF-related signalling was strongly positively correlated with ULBP expression across various endothelial subclusters in patients with SAP (figure 4O and online supplemental figure S6B–D). To experimentally assess this, we stimulated MS1 ECs with key cytokines involved in AP (TNF-α, IL-6, IL-1β and interferon-gamma (IFN-γ)) and found that TNF-α most potently upregulated *ULBP1* expression (figure 4P and online supplemental figure S6E–G).

Analysis of local TNF-α production in patients with SAP revealed upregulated *TNF* expression in nearly all cell populations. However, monocytes and macrophages were identified as the primary sources of elevated local *TNF* expression (online supplemental figure S6H,I). Subtype analysis revealed that two monocyte subsets and two macrophage subsets (Macro_CXCL3 and Macro_CX3CR1) expressed high levels of *TNF* (online supplemental figure S6J). Notably, the proinflammatory macrophage (Macro_CXCL3) was significantly upregulated in SAP (figure 3B).

Gut: first published as 10.1136/gutjnl-2025-337183 on 3 June 2026. Downloaded from http://gut.bmj.com/ on June 29, 2026 by guest. Protected by copyright, including for uses related to text and data mining, AI training, and similar technologies.

To determine the cell-type specificity of TNF-α signalling, we analysed TNF receptor expression across pancreatic cell subsets in patients with SAP. Among parenchymal cells, all EC subsets predominantly expressed *TNFR1*, with the highest expression observed in capillary. In contrast, other parenchymal cells (acinar, ductal, endocrine) primarily expressed *TNFR2* (online supplemental figure S7A). Consistent with this receptor distribution, in vitro stimulation with TNF-α induced *ULBP1* upregulation specifically in ECs (online supplemental figure S7B). To mechanistically dissect this endothelial-specific response, we employed human umbilical vein endothelial cells as a model system, chosen for their high transcriptomic concordance with human pancreatic ECs (online supplemental figure S7C). CRISPR-Cas9 knockout of TNF receptors in human umbilical vein endothelial cells demonstrated that loss of *TNFR1*—but not *TNFR2*—markedly blunted TNF-α-induced *ULBP1* upregulation, identifying TNFR1 as the dominant receptor of this endothelial response (online supplemental figure S7D).

To investigate the role of endothelial TNFR1 in SAP, MS1 ECs were pretreated with TNF-α and subsequently co-cultured with primary $CD8^+$ T cells isolated from SAP mice. TNFR1 knockout markedly attenuated $CD8^+$ T cell-mediated cytotoxicity, while significantly improving tube formation capacity and increasing the expression of key components of endothelial tight and adherens junctions that maintain barrier integrity (online supplemental figure S7E–I). Consistently, antibody-mediated blockade of TNFR1 in primary pancreatic ECs also conferred resistance to $CD8^+$ T-mediated cytotoxicity (online supplemental figure S7J). To verify TNFR1's role in vivo, we established a mouse model with pancreas endothelial-specific TNFR1 knockdown using adeno-associated virus serotype 9 carrying TNFR1-short hairpin RNA under the control of the TIE2 promoter, delivered via tail vein injection (online supplemental figure S7K,L). Following repeated SAP induction, TNFR1 knockdown significantly alleviated disease severity, reduced both local and systemic lactate levels, and improved pancreatic perfusion (online supplemental figure S7M–S). These results demonstrate that TNFR1 plays a critical role in mediating endothelial injury and microvascular dysfunction in SAP.

To elucidate the mechanism of endothelial *ULBP1* upregulation, we first employed Single-Cell rEgulatory Network Inference and Clustering analysis to compare ECs with high versus low ULBP1 expression, identifying candidate transcription factors (online supplemental figure S8A). Subsequent functional small interfering RNA screening of candidate genes identified activating transcription factor 4 (ATF4) as a key regulator of endothelial ULBP1 expression. Knockdown of ATF4 markedly blunted TNF-α-induced ULBP1 expression in ECs (online supplemental figure S8B). Consistently, ATF4, a key mediator of endoplasmic reticulum (ER) stress, was markedly increased in pancreatic ECs in a murine SAP model (online supplemental figure S8C).

Pathway analyses further revealed robust activation of ER stress and the integrated stress response (ISR) in ECs of patients with SAP (online supplemental figure S8D). In vitro, TNF-α stimulation of HUVECs activated the PERK–eIF2α axis, a core ISR pathway, leading to pronounced ATF4 induction (online supplemental figure S8E). Pharmacological induction of ER stress using thapsigargin (Tg) similarly increased ATF4 and ULBP1 expression, whereas inhibition of eIF2α signalling with ISRIB effectively reversed TNF-α-induced and Tg-induced upregulation of ATF4 and ULBP1 (online supplemental figure S8F,G). Together with prior evidence that ATF4 directly transcriptionally regulates ULBP1,[44] these findings establish that ATF4, induced via the TNF-α–PERK–eIF2α axis, serves as a central regulator of endothelial ULBP1 expression during SAP.

Serum TNF-α as an indicator of microcirculatory failure and prognosis in SAP

To investigate the correlations among TNF-α levels, EC damage and disease severity in patients with SAP, we stratified the eight patients with SAP from our scRNA-seq cohort into high (≥20, n=*3*) and low (<20, n=*5*) APACHE II score groups based on initial ICU assessments. The APACHE II score is a standard clinical tool used to evaluate disease severity and predict prognosis in patients with SAP. Acinar cells from patients with high APACHE II scores had significantly elevated hypoxia scores (figure 5A). Concurrently, ECs from these patients displayed enhanced apoptosis (figure 5B) and a marked upregulation of *ULBP1* (figure 5C). Moreover, pancreatic $CD8^+$ T cells in patients with high APACHE II scores also displayed increased activation and cytotoxicity (online supplemental figure S9A, eg, *NKG7*, *GZMK*, *GZMA*). These findings suggest that ULBPs signalling and subsequent $CD8^+$ T cell activation are associated with the severity of endothelial injury and overall disease progression in SAP.

To validate these findings clinically, we enrolled 153 newly diagnosed patients with SAP between 2021 and 2024 in our centre. We recorded the initial APACHE II scores, collected serum samples on admission and measured TNF-α alongside key SAP-related cytokine levels, including IL-6, IL-1β and IFN-γ.[45] In parallel, we measured serum levels of von Willebrand factor (vWF), E-selectin and angiopoietin-2 (ANG-II), which are established markers of endothelial damage. Correlation analyses were conducted among APACHE II scores, EC injury markers and cytokine levels (figure 5D).[16] Notably, only TNF-α showed a significant positive correlation with APACHE II scores (p=0.047; figure 5E). Moreover, TNF-α demonstrated the strongest association with all EC damage markers, notably vWF (R=0.341, p<0.001; figure 5F and online supplemental figure S9B), underscoring its utility as a potential biomarker for endothelial damage.

To objectively evaluate local pancreatic perfusion in patients with SAP, we developed a contrast-enhanced CT-based model that quantifies perfusion by calculating the ratio of pancreatic CT attenuation values to those of the abdominal aorta across different imaging phases (figure 5G). Notably, a statistically significant impairment in pancreatic perfusion was observed exclusively during the arterial phase using this model (online supplemental figure S9C). We subsequently performed correlation analysis between the arterial phase CT perfusion ratio and key serum cytokine levels. Among all cytokines tested, only TNF-α showed a significant negative correlation with the perfusion ratio (p=0.037; figure 5H and online supplemental figure S9D), highlighting its pivotal role in pancreatic microcirculatory impairment during SAP.

To determine whether the association between serum TNF-α and disease severity was independent of established prognostic factors, we performed a multivariable logistic regression analysis. The model was adjusted for the APACHE II score, vascular injury markers (vWF, ANG-II, E-selectin) and disease aetiology (online supplemental figure S9E). This analysis confirmed that a higher admission level of TNF-α was independently associated with an increased risk of death (OR=1.05, p=0.043). Notably, the APACHE II score also retained its strong independent predictive value (p=0.003), indicating that the prognostic information provided by TNF-α is complementary to, rather than redundant with, this composite severity score. The predictive performance

Gut: first published as 10.1136/gutjnl-2025-337183 on 3 June 2026. Downloaded from http://gut.bmj.com/ on June 29, 2026 by guest. Protected by copyright, including for uses related to text and data mining, AI training, and similar technologies.

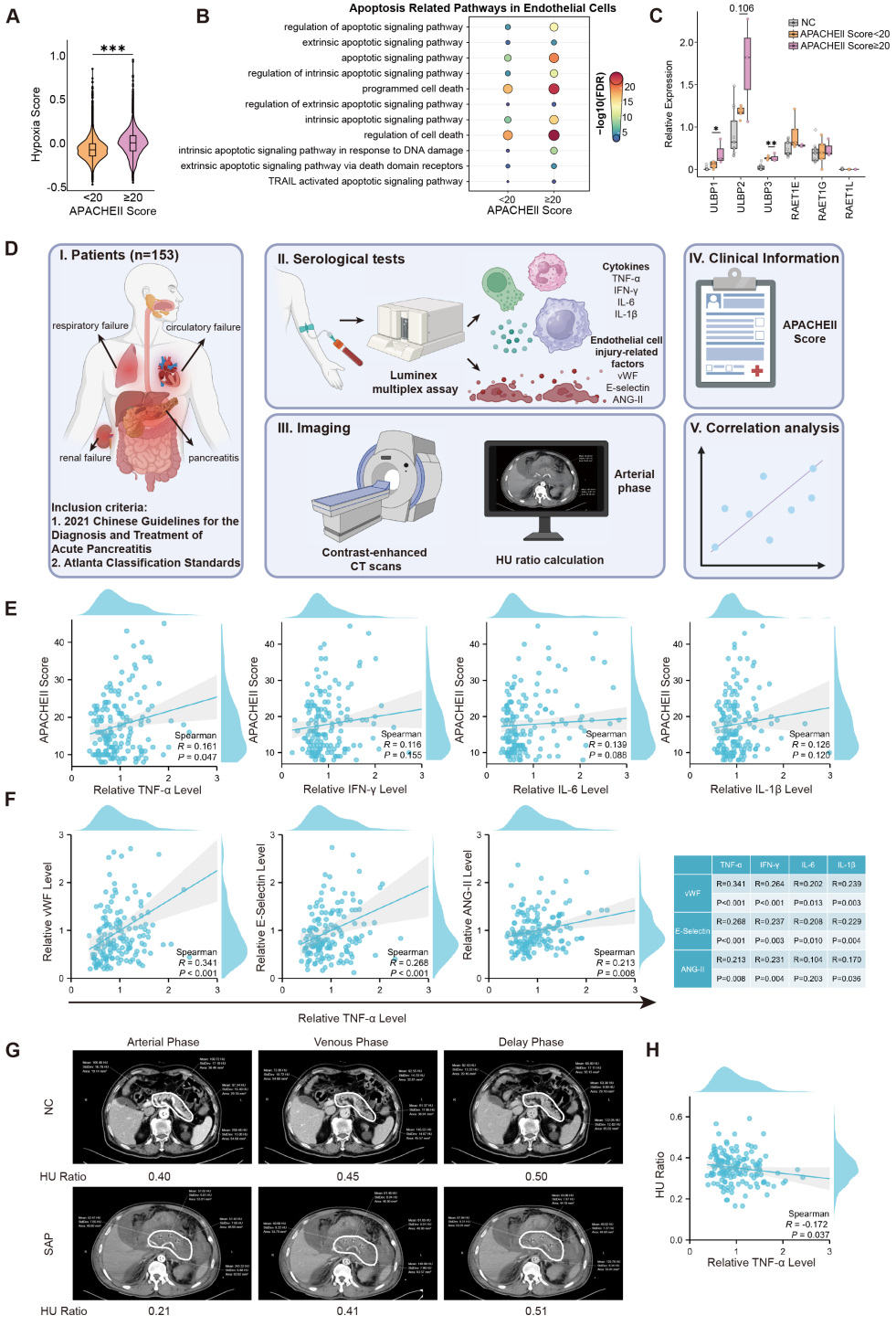

Figure 5 Serum TNF-α as a biomarker of pancreatic microcirculation and prognosis in SAP. (A) scRNA-seq indicated the higher hypoxia score of acinar cells from patients with SAP with APACHE II score ≥20 vs <20 (***p<0.001, Wilcoxon rank-sum test). (B) Dotplot of apoptosis related pathways (GO enrichment analysis) in ECs of patients with SAP stratified by APACHE II score (≥20 vs <20). (C) Boxplot of expression level of ULBP family genes for ECs in NC versus SAP (APACHE II score ≥20 vs <20) (*p<0.05, **p<0.01, Wilcoxon rank-sum test). (D) Schematic of the serum collection and molecular profiling in patients with SAP. (E) Spearman correlation analysis between relative TNF-α, IFN-γ, IL-6 and IL-1β level and APACHE II score of patients. (F) Spearman correlation analysis between relative TNF-α level and relative endothelial injury-related factors level (vWF, E-selectin and ANG-II) in serum. The table lists R values and p values. (G) Establishment of a contrast-enhanced CT model for evaluating pancreatic microcirculatory perfusion. A quantitative model was developed based on contrast-enhanced CT to assess microcirculatory perfusion in the pancreas. The HU ratio was defined as the ratio of the CT attenuation value of the pancreas to that of the abdominal aorta during different enhancement phases (see online supplemental methods for a detailed explanation). The area outlined in white indicates the radiologically recognisable pancreatic region. (H) Spearman correlation between relative TNF-α level in serum and HU ratio (pancreas/abdominal aorta) during the arterial phase of enhancement CT scan. ANG-II, angiopoietin-2; APACHE II, acute physiology and chronic health evaluation II; ECs, endothelial cells; FDR, false discovery rate; GO, Gene Ontology; HU, Hounsfield units; IFN-γ, interferon-gamma; IL, interleukin; NC, normal control; SAP, severe acute pancreatitis; scRNA-seq, single-cell RNA sequencing; TNF-α, tumour necrosis factor-alpha; ULBP, UL16-binding protein; vWF, von Willebrand factor.

Gut: first published as 10.1136/gutjnl-2025-337183 on 3 June 2026. Downloaded from http://gut.bmj.com/ on June 29, 2026 by guest. Protected by copyright, including for uses related to text and data mining, AI training, and similar technologies.

of a model incorporating TNF-α was robust, with an area under the receiver operating characteristic curve of 0.759 and a precision-recall curve-area under the curve of 0.716 (online supplemental figure S9F,G). The model was well-calibrated, demonstrating a strong agreement between predicted probabilities and observed outcomes (online supplemental figure S9H). These results establish admission TNF-α as an independent predictor of severity in SAP, providing additive value to conventional scoring systems.

In summary, TNF-α levels were strongly associated with both the degree of pancreatic microcirculatory disturbance and established clinical prognostic scores, suggesting that TNF-α is a promising therapeutic target for improving outcomes in SAP.

Therapeutic targeting of TNF-α effectively attenuates SAP in preclinical models

To evaluate whether anti-TNF-α therapy could improve treatment efficacy in SAP, we administered antimouse TNF-α antibodies in a continuous injection-induced SAP mouse model, alongside anti-CD8 antibody and sham-treated control groups (figure 6A; n=15 per group). As expected, mice treated with either anti-TNF-α or anti-CD8 antibodies exhibited reduced weight loss and lower mortality rates (figure 6B,C). Moreover, compared with the controls, both treatment groups demonstrated improved mobility compared with controls, indicating an overall alleviation of disease severity (figure 6D and online supplemental videos 1–3).

After 8 days of observation, the surviving mice were sacrificed for further analysis. Histological scoring revealed significant reductions in pancreatic oedema, necrosis and immune infiltration in both treatment groups (figure 6E). Serum analyses confirmed corresponding decreases in amylase, IL-6 and IL-1β levels (figure 6F–H). The anti-TNF-α group exhibited marked downregulation of membrane-bound ULBP1 expression on pancreatic ECs ($p<0.001$), suggesting endothelial protection via TNF-α blockade (figure 6I). Notably, ULBP1 expression was also reduced in the anti-CD8 group (figure 6I), implying that $CD8^+$ T cell-induced endothelial damage may further amplify the NKG2D–ULBPs axis. Additionally, both treatment groups showed decreased serum and pancreatic lactate levels, indicating improved tissue oxygenation and perfusion (figure 6J,K). These findings were further supported by LSCI, which confirmed that both anti-TNF-α or anti-CD8 therapy effectively preserved pancreatic microcirculation and enhanced perfusion in SAP mice ($p<0.05$; figure 6L).

To evaluate the clinical translatability of targeting TNF-α, we established a large-animal model of SAP using Panamanian piglets. Porcine SAP model was induced via surgical retrograde injection of sodium taurocholate into the pancreatic duct (figure 6M; n=3 per group). Successful model establishment was confirmed by histopathological findings, including local pancreatic necrosis, pulmonary congestion and extensive inflammatory cell infiltration in the lungs (figure 6N). Concurrently, serum levels of amylase and C-reactive protein (CRP) in peripheral blood were significantly elevated (figure 6O,P).

Next, we administered a single dose of infliximab, a clinically approved monoclonal antibody against TNF-α used to treat IBD,[46] in pigs with SAP and observed them for 1 week. The results demonstrated marked improvement in pancreatic and pulmonary pathology in the treatment group (figure 6N). Compared with those in the sham group, peripheral blood amylase and CRP levels were significantly lower (figure 6O,P). More importantly, serum lactate in the treatment group was markedly decreased, indicating improved systemic tissue perfusion (figure 6Q).

The aforementioned findings highlight a promising therapeutic avenue for the clinical management of SAP. In animal models, both TNF-α inhibition and $CD8^+$ T cell suppression have been shown to have significant protective effects. Given the widespread clinical application of anti-TNF therapies (eg, infliximab, adalimumab) in treating inflammatory conditions such as IBD, these approved agents offer new hope amidst the current lack of effective targeted treatments for AP.

DISCUSSION

In recent years, the incidence of SAP has steadily increased, imposing a significant burden on healthcare systems.[47] Currently, treatment for early-phase SAP remains largely supportive and includes organ support therapy, fluid resuscitation, pain control and nutritional management.[5] While advancements in surgical and endoscopic debridement have markedly reduced mortality in cases of severe necrosis and infection,[48] the lack of targeted therapeutics capable of actively intervening in the underlying pathophysiological processes continues to limit improvements in mortality rates, hospital stay durations and overall treatment costs. A major barrier to therapeutic innovation is the incomplete understanding of SAP mechanisms.

To address this, we established the first single-cell transcriptomic atlas of SAP by obtaining pancreatic tissues from critically ill patients undergoing necessary surgical interventions. This rare and valuable resource enabled the construction of the most detailed cellular landscape of human AP to date (figure 6R), and is publicly accessible via an interactive web portal. However, due to the inherent constraints related to sampling timing, this landscape does not capture the initiating events of SAP onset, but rather reflects the immune and stromal landscape under a sustained inflammatory state in pancreas. Our analysis revealed a central role for $CD8^+$ T cells in driving microvascular injury, resulting in pancreatic microcirculatory failure. This pathological process is orchestrated by the TNF-α/NKG2D/ULBPs signalling axis, highlighting a promising target for clinical intervention. Previous studies have reported that $CD8^+$ T cells target ECs under conditions such as chronic obstructive pulmonary disease and kidney transplantation.[49 50] Our findings support these observations by revealing the cytotoxic activity of activated $CD8^+$ T cells against ECs in SAP. Specifically, the upregulation of ULBPs on ECs further stimulates $CD8^+$ T cell activation, amplifying local endothelial injury as these cells circulate and infiltrate the pancreatic microvasculature. Although the availability of human SAP pancreatic tissues is relatively small with potential clinical heterogeneity, the key role of the NKG2D/ULBPs axis was consistently recapitulated across multiple experimental systems, including different animal models, *in vivo* and *in vitro* functional assays, as well as publicly available single-cell datasets from murine AP. Together, these convergent lines of evidence strengthen the robustness and generalisability of our conclusions.

Investigation of upstream regulators within our large human SAP cohort confirmed that TNF-α is the key mediator of this axis. Although other inflammatory cytokines are also associated with endothelial injury, TNF-α demonstrated the strongest correlation with microcirculatory disturbances, as evidenced by contrast-enhanced CT perfusion analysis and APACHE II severity scores. Furthermore, anti-TNF-α treatment showed therapeutic efficacy in both murine and porcine SAP models.

During the early systemic inflammatory response phase of SAP, extensive pancreatic necrosis establishes a trajectory

Gut: first published as 10.1136/gutjnl-2025-337183 on 3 June 2026. Downloaded from http://gut.bmj.com/ on June 29, 2026 by guest. Protected by copyright, including for uses related to text and data mining, AI training, and similar technologies.

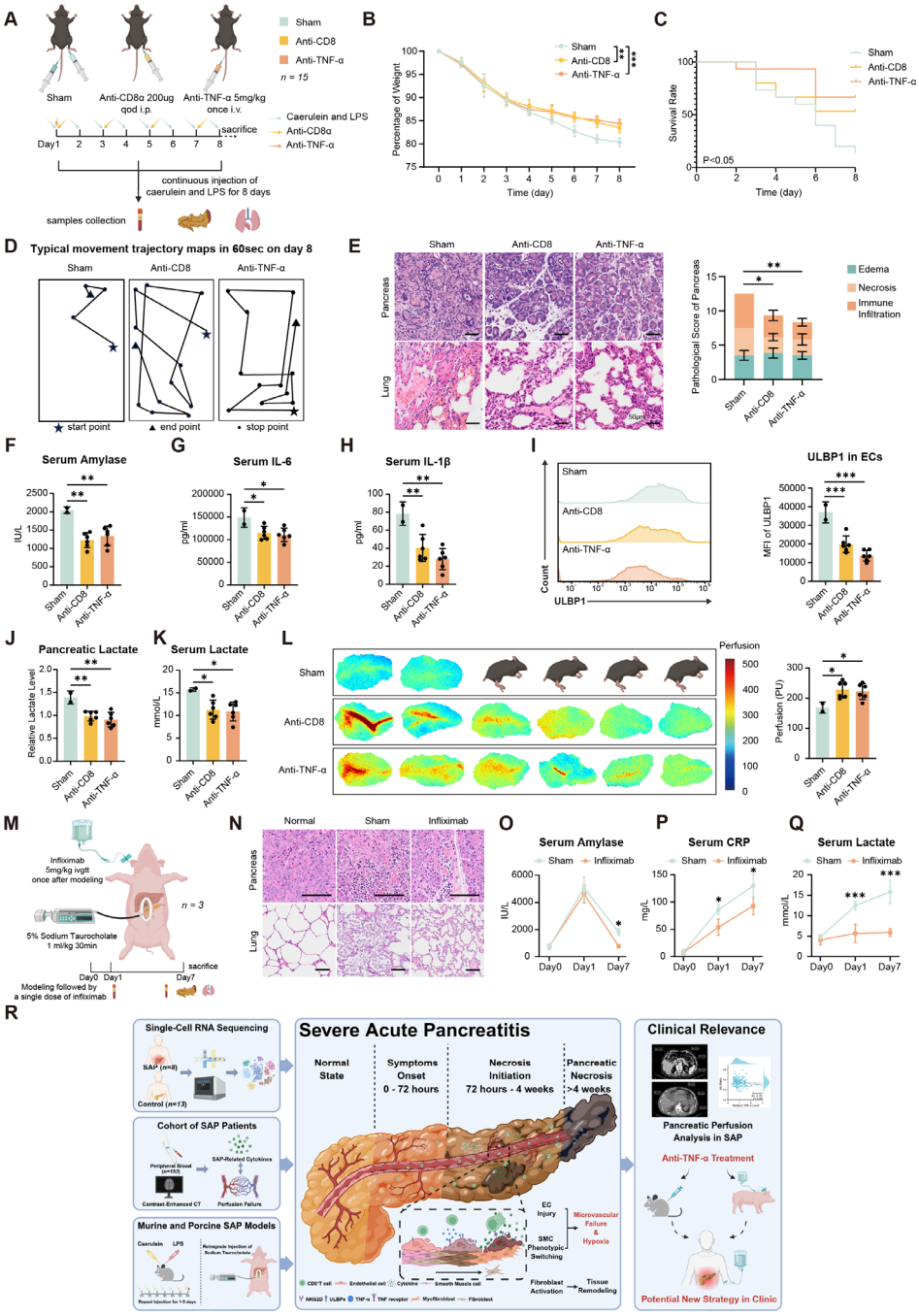

Figure 6 Therapeutic targeting of TNF-α effectively attenuates severe acute pancreatitis in preclinical models. (A) Schematic of anti-TNF-α and anti-CD8 monoclonal antibody treatment in C57BL/6 mice. (B) Body weight changes of mice in treatment versus sham group (n=15, mean±SD, **p<0.01, ***p<0.001, two-way ANOVA test). (C) Kaplan-Meier curves showing overall survival of 15 mice in monoclonal antibody treatment experiment followed up to 8 days (*p<0.05, Gehan-Breslow test). (D) Movement trajectory maps within 60 s for mice in each group. (Pentagram: start point; Triangle: end point; Dot: pause point; Lines: locomotion trajectory.). (E) Representative H&E images of pancreas (up panel) and lung (down panel) in each group (left panel) and subjected to histological score quantitative analysis (right panel, mean±SD, *p<0.05, **p<0.01, one-way ANOVA test). (Scale bars, 50 μm.). (F–H) Serum amylase (F), IL-6 (G) and IL-1β(H) in each group (mean±SD, *p<0.05, **p<0.01, ***p<0.001, one-way ANOVA test). (I) Mean Fluorescence Intensity of ULBP1 in ECs ($CD45^{-}CD31^{+}$) in mouse pancreas tissue between each group detected by flow cytometry (left panel) and quantitative analysis (right panel) (mean±SD, ***p<0.001, one-way ANOVA test). (J) The relative lactate level in mouse pancreas in each group. The relative lactate level was defined as the ratio between the concentration of lactate and total protein in pancreas (mean±SD, **p<0.01, one-way ANOVA test). (K) Serum lactate in each group (mean±SD, *p<0.05, one-way ANOVA test). (L) The image of LSCI of pancreatic microcirculation (left panel) and perfusion quantification (right panel, mean±SD, *p<0.05, one-way ANOVA test). (M) Schematic of the SAP model and Infliximab treatment experiment in porcine. (N) Representative H&E images of pancreas (up panel) and lung (down panel) in each group in porcine (Scale bars, 100 μm). (O–Q) Serum amylase (O), CRP (P) and IL-6 (Q) in each group in porcine (n=3, mean±SD, *p<0.05, ***p<0.001, two-way ANOVA test). (R) Graphical abstract of overall project. ANOVA, analysis of variance; CRP, C-reactive protein; ECs, endothelial cells; IL, interleukin; i.p., intraperitoneal; i.v., intravenous; LPS, lipopolysaccharide; LSCI, laser speckle contrast imaging; MFI, mean fluorescence intensity; PU, perfusion units; SAP, severe acute pancreatitis; SMC, smooth muscle cell; TNF-α, tumour necrosis factor-alpha; ULBP1, UL16-binding protein 1.

Gut: first published as 10.1136/gutjnl-2025-337183 on 3 June 2026. Downloaded from http://gut.bmj.com/ on June 29, 2026 by guest. Protected by copyright, including for uses related to text and data mining, AI training, and similar technologies.

toward subsequent infection and life-threatening complications.[51] Although early fluid resuscitation may offer certain benefits, it often fails to prevent the progression to infected necrosis and related complications.[13] Moreover, systemic anti-inflammatory therapy has long been a topic of interest in pancreatitis management, although its clinical application has remained largely confined to autoimmune pancreatitis.[52] Our study establishes a direct mechanistic link between TNF-α and $CD8^+$ T cell-mediated endothelial injury and microcirculatory disruption in SAP. Given the extensive clinical experience with anti-TNF-α agents in IBD, our findings pave the way for repurposing these therapies in SAP. Our animal data, together with reanalysis of data from previous studies, suggest that the TNF-α–NKG2D–ULBP axis is likely activated as early as 24–48 hours, followed by endothelial injury and microcirculatory dysfunction. Meanwhile, the sustained course of SAP is associated with an increased risk of infection. Given the essential role of TNF-α in host defence, anti-TNF-α therapy may increase the risk of severe infection in patients with SAP. Therefore, we propose that the optimal therapeutic window may lie within the early phase of disease (24–72 hours). Nevertheless, the optimal dosing strategy and therapeutic time window for anti-TNF-α intervention in SAP must be carefully determined in well-designed clinical trials.

Chronic pancreatitis (CP) is a well-established precancerous condition of pancreatic ductal adenocarcinoma (PDAC).[53] On the basis of our findings, SAP also exhibits several features suggestive of progression toward CP or even carcinogenesis. One of these features is ADM, a process whereby pancreatic acinar cells transdifferentiate into a duct-like phenotype in response to inflammation and injury. Animal models have demonstrated that ADM is particularly prominent in AP and SAP, where it is recognised as a precursor lesion for PDAC and a key source of pancreatic intraepithelial neoplasia.[7] In this study, we provide direct evidence of ADM in human SAP tissues.

In parallel, we observed that pancreatic fibroblasts in SAP adopt both profibrotic and tissue-remodelling phenotypes, indicating sustained activation during tissue repair.[27] In murine AP models, fibroblast activation occurs within hours of disease onset to initiate rapid tissue regeneration, a dynamic process rarely captured in human studies.[7] Our comprehensive single-cell transcriptomic atlas of human SAP helps bridge this translational gap, offering valuable insights into the molecular continuum connecting AP, CP and PDAC.

Author affiliations
[1]Department of General Surgery, Zhejiang University School of Medicine Sir Run Run Shaw Hospital, Hangzhou, Zhejiang, China
[2]Zhejiang Key Laboratory of Precise Diagnosis and Treatment of Abdominal Infection, Sir Run Run Shaw Hospital, School of Medicine, Zhejiang University, Hangzhou, Zhejiang, China
[3]Zhejiang Key Laboratory of Precision Diagnosis and Therapy for Major Gynecological Diseases, Women's Hospital School of Medicine Zhejiang University, Hangzhou, Zhejiang, China
[4]Department of Oncology, Zhejiang University School of Medicine Sir Run Run Shaw Hospital, Hangzhou, Zhejiang, China
[5]Department of Critical Care Medicine, Zhejiang University School of Medicine Sir Run Run Shaw Hospital, Hangzhou, Zhejiang, China
[6]Anhui Province Key Laboratory of Medical Physics and Technology, Institute of Health and Medical Technology, Chinese Academy of Sciences Hefei Institutes of Physical Science, Hefei, Anhui, China
[7]Institute of Immunology, Zhejiang University School of Medicine, Hangzhou, Zhejiang, China
[8]Department of Anesthesiology, Zhejiang University School of Medicine Sir Run Run Shaw Hospital, Hangzhou, Zhejiang, China
[9]Institute of Genetics, Zhejiang University School of Medicine, Hangzhou, Zhejiang, China

Correction notice This article has been corrected since it published Online First. The y-axis labels in figures 1-3 have been corrected.

Acknowledgements The authors appreciate Dr Xiaozhe Shi (Department of Radiology, Sir Run Run Shaw Hospital, School of Medicine, Zhejiang University) for her contribution to the interpretation of patient CT images, and Dr Zhiyao Xu (Department of Pathology, Sir Run Run Shaw Hospital, School of Medicine, Zhejiang University) for her assistance in pathological interpretation. The authors also appreciate Qingfu Yi and the team at LC Bio Technology for their assistance with sequencing. The authors carefully reviewed and revised the output to ensure both scientific accuracy and precision, and they take full responsibility for the final content of this publication. The authors sincerely acknowledge BioRender (www.biorender.com) for providing the platform used to create the schematic overview featured in this study.

Contributors HY, JQ, LS and WL conceived and designed the research. LS and WL performed most of the biochemical and molecular experiments, with assistance from BL, CJ, LM, BD, LD and ZP. DC performed all analyses of the single-cell RNA sequencing data under supervision of JQ, with assistance from QL. WL, ZH, XY and BS collected and provided clinical samples and data. LH, MC, JX, RB, HG and DW provided expertise, essential material. LS, WL and DC wrote the manuscript, HY, JQ, BS and XY revised the manuscript. All authors read and approved this version of the manuscript. During the preparation of this manuscript, the authors employed the GPT-4 model as a tool to enhance the clarity and readability of the original text, which was entirely drafted by the first author. The authors carefully reviewed and revised the output to ensure both scientific accuracy and precision, and they take full responsibility for the final content of this publication.

Funding The study was supported by the National Natural Science Foundation of China (No. 82470669/82270670 to HY, 82372856 to JQ, 82203426/82472742 to LS), The Central Government Guides Local Science and Technology Development Fund Projects (No. 2024ZY01020 to HY), Co-construction Science and Technology Program of Zhejiang Traditional Chinese Medicine Administration (No. GZY-ZJ-KJ-24032 to HY), Zhejiang Provincial Key Discipline Construction in Traditional Chinese Medicine (No.2024-XK-46 to HY), The Key Scientific Research Program of Hangzhou (No. 2024SZD1B06 to HY), The Huadong Medicine Joint Fund of Zhejiang Provincial Natural Science Foundation of China (No. LHDMD25H030001 to HY). Zhejiang Province Key Research and Development Program (No. 2024C03239 to JQ, 2025C02133 to XY, 2024C03201 to BS), Zhejiang Natural Science Foundation (No. LY23H160021/MS26H160105 to LS), Fundamental Research Funds for the Zhejiang Provincial Universities (No. 226-2023-00011 to LS), Clinical Top-notch Personnel Support of Zhejiang University (LS), China Postdoctoral Science Foundation (No. 2024M752826 to DC).

Competing interests None declared.

Patient and public involvement Patients and/or the public were not involved in the design, or conduct, or reporting, or dissemination plans of this research.

Patient consent for publication Not applicable.

Ethics approval This study involves human participants and was approved by Sir Run Run Shaw Hospital, Zhejiang University School of Medicine Ethics Committee. The approval number is 2022Yan0142. Participants gave informed consent to participate in the study before taking part.

Provenance and peer review Not commissioned; externally peer reviewed.

Data availability statement Data are available upon reasonable request. The raw sequencing data generated in this study have been deposited in the National Genomics Data Center (NGDC) under BioProject accession number PRJCA044769 (Genome Sequence Archive for Human: HRA012835). Data are accessible through the Human Genetic Resources Service System of the Ministry of Science and Technology, China, following a standard application process. Public scRNA-seq data reanalysed in this study are available under NGDC BioProject accession PRJCA001063 and GEO accession GSE235874. Processed scRNA-seq data (raw count matrices) for all samples are hosted on an interactive web server for the single-cell SAP atlas (https://atlas.qian-lab.org/sap), which enables in-depth data exploration and visualisation. Code generated for this study is available on GitHub (https://github.com/Qian-Laboratory/SAP-atlas-paper-2025).

Supplemental material This content has been supplied by the author(s). It has not been vetted by BMJ Publishing Group Limited (BMJ) and may not have been peer-reviewed. Any opinions or recommendations discussed are solely those of the author(s) and are not endorsed by BMJ. BMJ disclaims all liability and responsibility arising from any reliance placed on the content. Where the content includes any translated material, BMJ does not warrant the accuracy and reliability of the translations (including but not limited to local regulations, clinical guidelines, terminology, drug names and drug dosages), and is not responsible for any error and/or omissions arising from translation and adaptation or otherwise.

Open access This is an open access article distributed in accordance with the Creative Commons Attribution Non Commercial (CC BY-NC 4.0) license, which

Gut: first published as 10.1136/gutjnl-2025-337183 on 3 June 2026. Downloaded from http://gut.bmj.com/ on June 29, 2026 by guest. Protected by copyright, including for uses related to text and data mining, AI training, and similar technologies.

permits others to distribute, remix, adapt, build upon this work non-commercially, and license their derivative works on different terms, provided the original work is properly cited, appropriate credit is given, any changes made indicated, and the use is non-commercial. See: https://creativecommons.org/licenses/by-nc/4.0/.

ORCID iDs
Boqiang Liu https://orcid.org/0000-0003-4214-4136
Rongpan Bai https://orcid.org/0000-0002-0687-2729
Hong Yu https://orcid.org/0000-0001-5990-3720

REFERENCES

1 van Dijk SM, Hallensleben NDL, van Santvoort HC, *et al*. Acute pancreatitis: recent advances through randomised trials. *Gut* 2017;66:2024–32.
2 Sendler M, Weiss F-U, Golchert J, *et al*. Cathepsin B-Mediated Activation of Trypsinogen in Endocytosing Macrophages Increases Severity of Pancreatitis in Mice. *Gastroenterology* 2018;154:704–18.
3 Bruce JIE, Sánchez-Alvarez R, Sans MD, *et al*. Insulin protects acinar cells during pancreatitis by preserving glycolytic ATP supply to calcium pumps. *Nat Commun* 2021;12:4386.
4 Kang H, Hu Q, Yang Y, *et al*. Urolithin A's Role in Alleviating Severe Acute Pancreatitis via Endoplasmic Reticulum-Mitochondrial Calcium Channel Modulation. *ACS Nano* 2024;18:13885–98.
5 Søreide K, Barreto SG, Pandanaboyana S. Severe acute pancreatitis. *Br J Surg* 2024;111.
6 Wu Z, Wang S, Wu Z, *et al*. Altered immune cell in human severe acute pancreatitis revealed by single-cell RNA sequencing. *Front Immunol* 2024;15:1354926.
7 Aney KJ, Jeong W-J, Vallejo AF, *et al*. Novel Approach for Pancreas Transcriptomics Reveals the Cellular Landscape in Homeostasis and Acute Pancreatitis. *Gastroenterology* 2024;166:1100–13.
8 Trepte CJC, Bachmann KA, Stork JH, *et al*. The impact of early goal-directed fluid management on survival in an experimental model of severe acute pancreatitis. *Intensive Care Med* 2013;39:717–26.
9 Eibl G, Buhr HJ, Foitzik T. Therapy of microcirculatory disorders in severe acute pancreatitis: what mediators should we block? *Intensive Care Med* 2002;28:139–46.
10 Cuthbertson CM, Christophi C. Disturbances of the microcirculation in acute pancreatitis. *Br J Surg* 2006;93:518–30.
11 Antkowiak R, Bialecki J, Chabowski M, *et al*. Treatment of Microcirculatory Disturbances in Acute Pancreatitis: Where Are We Now? *Pancreas* 2022;51:415–21.
12 Tomkötter L, Erbes J, Trepte C, *et al*. The Effects of Pancreatic Microcirculatory Disturbances on Histopathologic Tissue Damage and the Outcome in Severe Acute Pancreatitis. *Pancreas* 2016;45:248–53.
13 de-Madaria E, Buxbaum JL, Maisonneuve P, *et al*. Aggressive or Moderate Fluid Resuscitation in Acute Pancreatitis. *N Engl J Med* 2022;387:989–1000.
14 Komara NL, Paragomi P, Greer PJ, *et al*. Severe acute pancreatitis: capillary permeability model linking systemic inflammation to multiorgan failure. *Am J Physiol Gastrointest Liver Physiol* 2020;319:G573–83.
15 Claesson-Welsh L, Dejana E, McDonald DM. Permeability of the Endothelial Barrier: Identifying and Reconciling Controversies. *Trends Mol Med* 2021;27:314–31.
16 Dumnicka P, Maduzia D, Ceranowicz P, *et al*. The Interplay between Inflammation, Coagulation and Endothelial Injury in the Early Phase of Acute Pancreatitis: Clinical Implications. *Int J Mol Sci* 2017;18:354.
17 Wang X, Guo Y, Cui T, *et al*. Telomerase reverse transcriptase restores pancreatic microcirculation profiles and attenuates endothelial dysfunction by inhibiting mitochondrial superoxide production: A potential target for acute pancreatitis therapy. *Biomed Pharmacother* 2023;167:115576.
18 Wang X, Cui T, Zhang T, *et al*. Angiotensin-(1-7) Restores Microcirculation Profiles in Acute Pancreatitis: Secret of Telomerase Reverse Transcriptase. *Pancreas* 2022;51:1047–55.
19 Peng J, Sun B-F, Chen C-Y, *et al*. Single-cell RNA-seq highlights intra-tumoral heterogeneity and malignant progression in pancreatic ductal adenocarcinoma. *Cell Res* 2019;29:725–38.
20 Sastre J, Pérez S, Sabater L, *et al*. Redox signaling in the pancreas in health and disease. *Physiol Rev* 2025;105:593–650.
21 Bopanna S, Nayak B, Prakash S, *et al*. Increased oxidative stress and deficient antioxidant levels may be involved in the pathogenesis of idiopathic recurrent acute pancreatitis. *Pancreatology* 2017;17:529–33.
22 Park M-J, Iyer S, Xue X, *et al*. HIF1-alpha Regulates Acinar Cell Function and Response to Injury in Mouse Pancreas. *Gastroenterology* 2018;154:1630–4.
23 Kong B, Bruns P, Behler NA, *et al*. Dynamic landscape of pancreatic carcinogenesis reveals early molecular networks of malignancy. *Gut* 2018;67:146–56.
24 Baldan J, Camacho-Roda J, Ballester M, *et al*. Resolution of Acinar Dedifferentiation Regulates Tissue Remodeling in Pancreatic Injury and Cancer Initiation. *Gastroenterology* 2024;167:718–32.
25 De Backer D, Orbegozo Cortes D, Donadello K, *et al*. Pathophysiology of microcirculatory dysfunction and the pathogenesis of septic shock. *Virulence* 2014;5:73–9.
26 Vallet B. Endothelial cell dysfunction and abnormal tissue perfusion. *Crit Care Med* 2002;30:S229–34.
27 Buechler MB, Pradhan RN, Krishnamurty AT, *et al*. Cross-tissue organization of the fibroblast lineage. *Nature New Biol* 2021;593:575–9.
28 Wirka RC, Wagh D, Paik DT, *et al*. Atheroprotective roles of smooth muscle cell phenotypic modulation and the TCF21 disease gene as revealed by single-cell analysis. *Nat Med* 2019;25:1280–9.
29 Gukovskaya AS, Gukovsky I, Algül H, *et al*. Autophagy, Inflammation, and Immune Dysfunction in the Pathogenesis of Pancreatitis. *Gastroenterology* 2017;153:1212–26.
30 Stojanovic B, Jovanovic IP, Stojanovic MD, *et al*. The Emerging Roles of the Adaptive Immune Response in Acute Pancreatitis. *Cells* 2023;12:1495.
31 Burger F, Baptista D, Roth A, *et al*. Single-Cell RNA-Seq Reveals a Crosstalk between Hyaluronan Receptor LYVE-1-Expressing Macrophages and Vascular Smooth Muscle Cells. *Cells* 2022;11:411.
32 Mayerle J, Sendler M, Hegyi E, *et al*. Genetics, Cell Biology, and Pathophysiology of Pancreatitis. *Gastroenterology* 2019;156:1951–68.
33 Wauters E, Van Mol P, Garg AD, *et al*. Discriminating mild from critical COVID-19 by innate and adaptive immune single-cell profiling of bronchoalveolar lavages. *Cell Res* 2021;31:272–90.
34 Bassez A, Vos H, Van Dyck L, *et al*. A single-cell map of intratumoral changes during anti-PD1 treatment of patients with breast cancer. *Nat Med* 2021;27:820–32.
35 Taflin C, Favier B, Baudhuin J, *et al*. Human endothelial cells generate Th17 and regulatory T cells under inflammatory conditions. *Proc Natl Acad Sci USA* 2011;108:2891–6.
36 Andersen BM, Faust Akl C, Wheeler MA, *et al*. Barcoded viral tracing identifies immunosuppressive astrocyte-glioma interactions. *Nature New Biol* 2025;644:1097–106.
37 Katzenelenbogen Y, Sheban F, Yalin A, *et al*. Coupled scRNA-Seq and Intracellular Protein Activity Reveal an Immunosuppressive Role of TREM2 in Cancer. *Cell* 2020;182:872–85.
38 Lerner EC, Woroniecka KI, D'Anniballe VM, *et al*. CD8$^+$ T cells maintain killing of MHC-I-negative tumor cells through the NKG2D-NKG2DL axis. *Nat Cancer* 2023;4:1258–72.
39 Balint E, Feng E, Giles EC, *et al*. Bystander activated CD8$^+$ T cells mediate neuropathology during viral infection via antigen-independent cytotoxicity. *Nat Commun* 2024;15:896.
40 Cadoux M, Caruso S, Pham S, *et al*. Expression of NKG2D ligands is downregulated by β-catenin signalling and associates with HCC aggressiveness. *J Hepatol* 2021;74:1386–97.
41 Pende D, Rivera P, Marcenaro S, *et al*. Major histocompatibility complex class I-related chain A and UL16-binding protein expression on tumor cell lines of different histotypes: analysis of tumor susceptibility to NKG2D-dependent natural killer cell cytotoxicity. *Cancer Res* 2002;62:6178–86.
42 Soriani A, Zingoni A, Cerboni C, *et al*. ATM-ATR-dependent up-regulation of DNAM-1 and NKG2D ligands on multiple myeloma cells by therapeutic agents results in enhanced NK-cell susceptibility and is associated with a senescent phenotype. *Blood* 2009;113:3503–11.
43 Lanier LL. NKG2D Receptor and Its Ligands in Host Defense. *Cancer Immunol Res* 2015;3:575–82.
44 Gowen BG, Chim B, Marceau CD, *et al*. A forward genetic screen reveals novel independent regulators of ULBP1, an activating ligand for natural killer cells. *Elife* 2015;4:e08474.
45 Chen S, Zhu J, Sun L-Q, *et al*. LincRNA-EPS alleviates severe acute pancreatitis by suppressing HMGB1-triggered inflammation in pancreatic macrophages. *Immunology* 2021;163:201–19.
46 Croft M, Salek-Ardakani S, Ware CF. Targeting the TNF and TNFR superfamilies in autoimmune disease and cancer. *Nat Rev Drug Discov* 2024;23:939–61.
47 Peery AF, Crockett SD, Murphy CC, *et al*. Burden and Cost of Gastrointestinal, Liver, and Pancreatic Diseases in the United States: Update 2021. *Gastroenterology* 2022;162:621–44.
48 Baron TH, DiMaio CJ, Wang AY, *et al*. American Gastroenterological Association Clinical Practice Update: Management of Pancreatic Necrosis. *Gastroenterology* 2020;158:67–75.
49 Villaseñor-Altamirano AB, Jain D, Jeong Y, *et al*. Activation of CD8$^+$ T Cells in Chronic Obstructive Pulmonary Disease Lung. *Am J Respir Crit Care Med* 2023;208:1177–95.
50 Tilly G, Doan-Ngoc T-M, Yap M, *et al*. IL-15 Harnesses Pro-inflammatory Function of TEMRA CD8 in Kidney-Transplant Recipients. *Front Immunol* 2017;8:778.
51 de-Madaria E, Buxbaum JL. Advances in the management of acute pancreatitis. *Nat Rev Gastroenterol Hepatol* 2023;20:691–2.
52 Masamune A, Nishimori I, Kikuta K, *et al*. Randomised controlled trial of long-term maintenance corticosteroid therapy in patients with autoimmune pancreatitis. *Gut* 2017;66:487–94.
53 Deng D, Begum H, Liu T, *et al*. NFAT5 governs cellular plasticity-driven resistance to KRAS-targeted therapy in pancreatic cancer. *J Exp Med* 2024;221:e20240766.

Gut: first published as 10.1136/gutjnl-2025-337183 on 3 June 2026. Downloaded from http://gut.bmj.com/ on June 29, 2026 by guest. Protected by copyright, including for uses related to text and data mining, AI training, and similar technologies.